

1 An improved modelling chain for bias-adjusted high-resolution 2 climate and hydrological projections for Norway

3 Shaochun Huang¹, Wai Kwok Wong¹, Andreas Dobler³, Sigrid Jørgensen Bakke¹, Stein Beldring¹,
4 Ingjerd Haddeland^{1*}, Hans Olav Hygen³, Tyge Løvset², Stephanie Mayer², Kjetil Melvold¹, Irene Brox
5 Nilsen¹, Gusong Ruan¹, Silje Lund Sørland^{2^}, Anita Verpe Dyrredal³

6 ¹Department of Hydrology, Norwegian Water Resources and Energy Directorate, Oslo, 0301, Norway

7 ²NORCE Research AS, and Bjerknes Centre for Climate Research, Bergen, 5008, Norway

8 ³Department of Climate and Environment, Norwegian Meteorological Institute, Oslo, 0371, Norway

9 [^]now at SWECO AS, Bergen, Norway

10 ^{*}now at Lyse AS, Stavanger, 4018, Norway

11 *Correspondence to:* Shaochun Huang (shh@nve.no)

12 **Abstract**

13 About every 10 years, the Norwegian Centre for Climate Services publishes a national climate assessment report, presenting
14 the updated historical climate change and climate projections towards the end of this century. This paper documents the model
15 experiment used to generate high-resolution climate and hydrological projections for the new climate assessment report
16 published in October 2025. The model experiment follows the standard modelling chain for hydrological impact assessment,
17 i.e., climate model selection - downscaling and bias adjustment - hydrological modelling. However, compared with the model
18 experiment for the climate assessment report published in 2015, all modelling components have been improved in terms of
19 data availability, data quality and methodology. Specifically, a large climate model ensemble was available and new criteria
20 were developed to select tailored climate projections for Norway. Two bias-adjustment methods (one univariate and one
21 multivariate) were applied to account for the uncertainty of method choice. The hydrological modelling was improved by
22 implementing a physically-based Penman-Monteith method for evaporation and a glacier model accounting for glacier retreat
23 under climate change scenarios. Besides model description, this paper elaborates the effects of different bias-adjustment
24 methods and the contribution of climate models and bias-adjustment methods to the uncertainty of climate and hydrological
25 projections under the RCP4.5 scenario as examples. The results show that the two bias-adjustment methods can contribute
26 larger uncertainty to seasonal projections than climate models. The multivariate bias-adjustment method improves hydrological
27 simulations, especially in the reference period, but cannot conserve climate change signals of the original climate projections.
28 The dataset generated by the presented modelling chain provides the most updated, comprehensive and detailed
29 hydrometeorological projections for mainland Norway, serving as a knowledge base for climate change adaptation to decision
30 makers at various administrative levels in Norway.

33 **1 Introduction**

34 It is unequivocal that human influence has warmed the climate at a rate that is unprecedented in at least the last 2000 years
35 (IPCC, 2021). The human-induced warming has already modified the global hydrological cycle, leading to significant shifts
36 in the spatial and temporal patterns of hydrological components (Gu and Adler, 2015; Gudmundsson et al., 2021; Li et al.,
37 2023) and more intensive and frequent hydroclimatic extreme events (Alifu et al., 2022; Chinita et al. 2021; Dunn et al., 2020;
38 Padrón et al., 2020). These impacts pose unprecedented challenges for water resource management at regional and local scales,
39 and they are expected to be more severe in the future if unsustainable development continues (Wang and Liu, 2023). Therefore,
40 understanding of the potential climate change impact from a long-term and systematic perspective serves as a key basis to
41 develop climate adaptation strategies, such as incorporating climate projections into European building standards (EEA, 2025)
42 and national climate risk adaptations (DCCEW, 2023).

43 General circulation models (GCMs) are important tools to understand and predict climate behavior under various greenhouse
44 gas emission scenarios on the global scale. GCMs have been developed rapidly in the last decades, with an increasing number
45 of models from over 40 within the Coupled Model Intercomparison Project phase 5 (CMIP5, Taylor et al., 2012) for
46 Representative Concentration Pathway (RCP) emission scenarios to over 60 within CMIP6 (Eyring et al., 2016) for the Shared
47 Socioeconomic Pathways (SSP) emission scenarios. Such a large ensemble of models provides valuable information of
48 uncertainty for future climate projections, accounting for natural climate variability, unknown socio-economic developments,
49 and model differences (Hawkins and Sutton, 2011). However, the use of the full ensemble can be challenging for impact
50 models due to computational restrictions, so it often requires a careful selection of projections for specific study areas based
51 on comprehensive analysis of the whole ensemble (Dalelane et al., 2018). In addition, GCM outputs are hardly applied for
52 impact assessment at regional and local scales due to their coarse spatial resolutions (e.g., ~ 0.25 to 3° for the CMIP6 models
53 and ~ 0.5 to 4° for the CMIP5 models) and systematic biases (Rössler et al., 2019), and they are usually downscaled to fine
54 spatial resolutions and bias adjusted for climate impact assessment and adaptation planning (Martinich and Crimmins, 2019).

55 The GCM outputs can be downscaled dynamically using regional climate models (RCMs) or statistically based on statistical
56 relationships between coarse-resolution variables in GCMs and fine-resolution or local observations in the historical period
57 (Zhang et al., 2020). Various RCMs and statistical downscaling methods have been developed and applied to downscale the
58 GCM outputs, increasing the number of climate projections for region scales. For example, the European Coordinated Regional
59 Downscaling Experiment (EURO-CORDEX, Jacob et al., 2020) applies 11 RCMs to downscale the outputs from 14 GCMs to
60 0.11° (ca. 12.5 km) horizontal resolution. Due to the high computational cost and time consumption, each RCM is able to
61 downscale one or a few GCMs outputs, resulting in 30, 25 and 64 regional climate projections for Europe under the RCP2.6,
62 RCP4.5 and RCP8.5 scenarios, respectively. In contrast, statistical downscaling methods, which are often combined with bias

63 adjustment, can be easily applied for a large ensemble of GCMs due to low computational requirements and fast calculations,
64 and over 50 statistical downscaling methods have been applied for Europe (Gutiérrez et al., 2019).

65 Each downscaling method has its strengths and weaknesses. The dynamic downscaling ensures the physical relationships
66 between climatic variables and spatial dependence, but it inherits significant biases from GCMs and requires further bias
67 adjustment and/or statistical downscaling depending on the scale of impact studies (Hundecha et al., 2016; Maraun og
68 Widmann, 2018). In contrast, the statistical downscaling usually outperforms the RCMs in terms of bias, but many methods
69 downscale individual climatic variables independently. As univariate bias-adjustment methods, this approach does not modify
70 inter-variable dependency structures but keeps them as in the original model data which can be inaccurate. Eum et al. (2020)
71 demonstrated different impact of univariate and multivariate statistical downscaling methods on reproduction of snowfall and
72 recommended the use of the multivariate methods for climate change impact assessment in snow-dominated watersheds. Meyer
73 et al. (2019) also found underestimation of snow accumulation (up to 50%) in alpine catchments when using univariate contra
74 multivariate bias-adjustment approach, which can be attributed to less precipitation below temperatures of 0 °C.

75 Due to the large number of GCM projections and downscaling methods, as well as their strengths and weaknesses, to construct
76 a downscaled and bias-corrected ensemble for specific regions is challenging. Different choices of GCM and downscaling
77 methods can lead to considerably different local climate projections and thus contribute large uncertainty to local decision-
78 relevant climate outcomes (Tang et al., 2016; Lafferty and Sriver, 2023). In addition, they result in different climate impact
79 projections for streamflow (Kay, 2025), flood hazard (Kundzewicz et al., 2017), agriculture (Li et al., 2023), ecosystem
80 (Pourmokhtarian et al., 2016), etc, causing inconsistent impact assessments not only within each impact sector but also across
81 sectors. Therefore, a consistent and tailored ensemble of regional climate projections is highly appreciated for each region and
82 many countries have put great efforts to create national ensembles of climate projections (Golding et al., 2025), such as
83 Switzerland (Fischer et al., 2022), Germany (Hübener et al., 2017), UK (Reyniers et al., 2025) and Australia (Peter et al.,
84 2024).

85 Norway is located in the northern high latitudes, which have experienced the strongest warming since 1980 among all regions
86 in the world, with warming trends spanning from 0.2 to more than 0.6 °C/decade (IPCC, 2021). The strong warming in the
87 historical period raises great attention from both the scientific community and the public to future climate change and its
88 impacts on hydropower production (about 90% of total power production in the country), winter tourism (skiing), and water
89 related natural hazards (i.e., flood, drought, avalanche and landslide). However, it is specifically challenging to construct robust
90 and reliable climate projections as well as hydrological impact projections in Norway, due to the high heterogeneity in
91 topographic and hydroclimatological characteristics.

92 Norway is one of the most mountainous countries in Europe, with more than 90% of the landscape consisting of mountains.
93 The rugged topography leads to a complex spatial and temporal pattern of temperature and precipitation, varying with

94 geographical position, elevation, aspect (slope direction), and slope angle (Dobrowski et al., 2009; Franke, 2024). The spatial
95 resolutions of the state-of-the-art GCMs and RCMs are too coarse to provide sufficient spatial variations of climate for such
96 complex terrain. In addition, these projections often show a cold bias for Norway (Wong et al., 2016), which for example leads
97 to a prolonged snow season, low winter runoff and late snowmelt in hydrological projections (Nilsen et al., 2021).

98 In order to construct a consistent and tailored ensemble of national climate projections as well as hydrological projections for
99 Norway, the Norwegian Centre for Climate Services (NCCS) brings together experts from the Norwegian Meteorological
100 Institute, the Norwegian Water Resources and Energy Directorate (NVE), the Norwegian Research Centre (NORCE) and
101 Bjerknes Centre for Climate Research. NCCS is responsible for the national climate assessment report, updated about every
102 10 years, which presents updated historical climate change and climate projections towards the end of this century and serves
103 as a knowledge base for climate change adaptation to decision makers and planners at various administrative levels in Norway
104 (Nilsen et al., 2022). The previous climate assessment report “Climate in Norway 2100” (Hanssen-Bauer et al., 2015; hereafter
105 abbreviated CiN-2015), published in 2015, was based on 10 available GCM-RCM combinations within the CMIP5 and EURO-
106 CORDEX frameworks. The projections were further re-gridded and bias-adjusted into 1×1 km resolution using empirical
107 quantile mapping and forced the distributed version of the HBV (Hydrologiska Byråns Vattenbalansavdelningen, i.e. “The
108 Hydrological Bureau’s Water Balance Department”) hydrological model (distHBV, Beldring et al., 2003) to generate
109 hydrological projections. This spatial resolution is the result of the need to serve projections that can be used locally on the
110 one hand, and availability of computational resources and reference datasets to produce daily maps for the whole of Norway
111 on the other. During the last 10 years, all methods along the modelling chain, including GCMs, RCMs, climate model
112 selections, statistical downscaling and bias correction, and hydrological models, have been further developed, and the
113 observation data has been updated and improved. These developments promote the new generation of high-resolution and
114 bias-adjusted climate and hydrological projections, which are more robust than the previous ones in CiN-2015.

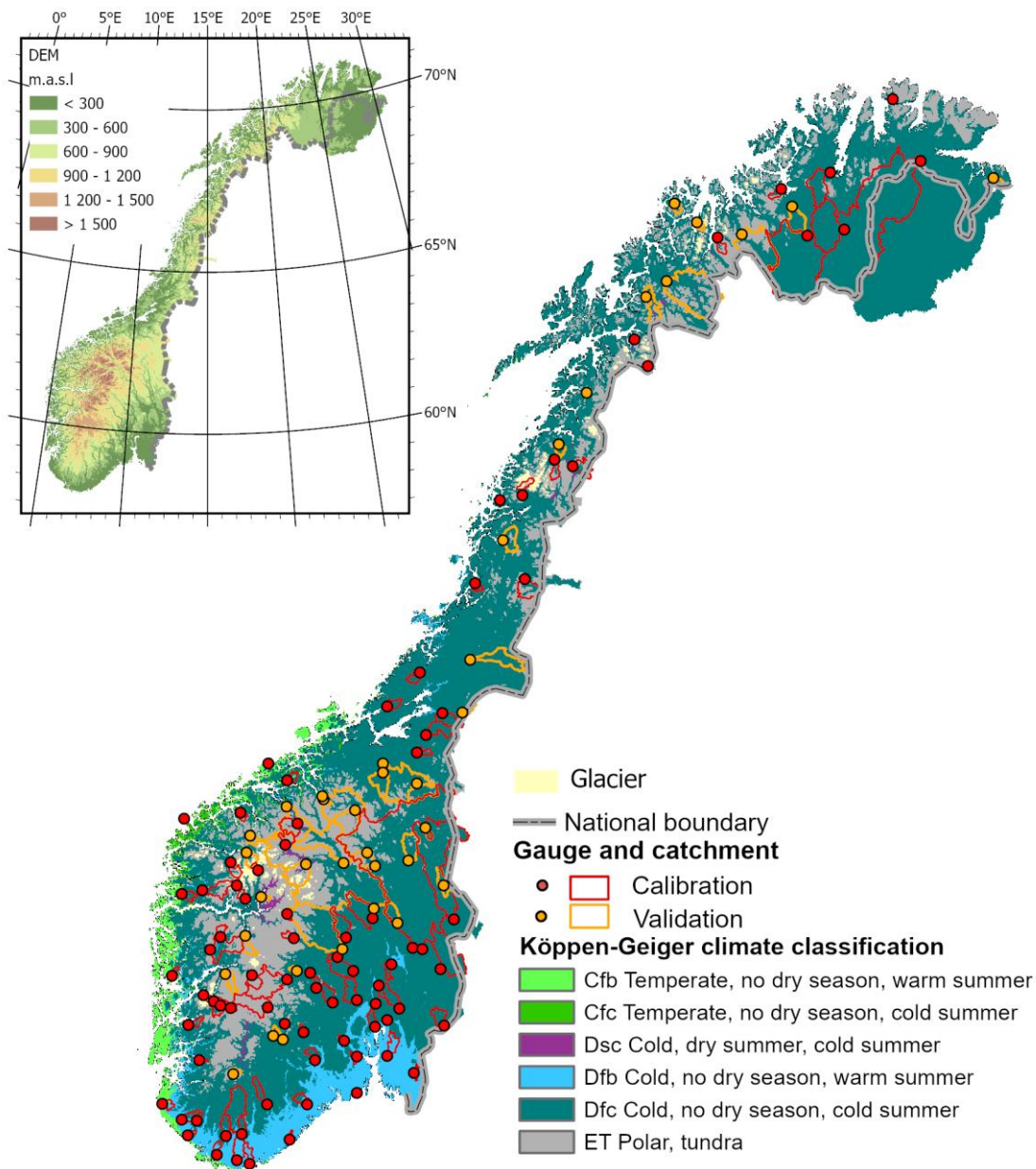
115 In this paper, we present the full description of the methods to produce the updated downscaled and bias-adjusted climate
116 projections and hydrological projections for the new climate assessment report for Norway “CiN-2025” (Dyrrdal et al., 2025),
117 specifically focusing on selection of GCM-RCMs combinations, statistical downscaling and bias-adjustment and hydrological
118 modelling. Section 2 introduces the study area and historical input data. The methods described include the overview of the
119 whole modelling chain (Section 3), selection of atmospheric variables from a set of EURO-CORDEX simulations (Section 4),
120 statistical downscaling and bias-adjustment method (Section 5) and hydrological modelling (Section 6). In Section 7 and 8,
121 we present the climate and hydrological products and uncertainty analysis. Finally, we discuss the limitations of the methods
122 and the potential applications of the products, and point out the way towards the next generation of national climate projections
123 for Norway in Section 9.

124 **2 Study area and historical data**

125 **2.1 Study area**

126 The modelling domain of this study is the mainland of Norway and a few river catchments draining from neighbouring
127 countries (Sweden and Finland) (Fig. 1), resulting in 354448 1x1 km² grid cells. Due to large variations in latitude and altitude,
128 Norway exhibits six climate regimes according to the Köppen-Geiger climate classification (Beck et al., 2018), ranging from
129 temperate climate along the west coast to polar climate in high mountains and in the north (Fig. 1). The average elevation of
130 Norway is about 460 m, ranging from 0 along the coast to 2469 m at Galdhøpiggen in the center of the country. Open firm
131 ground and forest are the two major land covers in Norway, accounting for 36% and 37.8% of the mainland area, respectively
132 (Statistics Norway, 2025). There are also large areas of bedrock (8.5%), followed by water (6.2%), bogs (5.4%), agricultural
133 land (3.5%) and built-up (1.7%). About 1% of mainland Norway is covered by glaciers (Fig. 1). The mean annual temperature
134 in the current standard normal period 1991–2020 ranges from -9.5 to +9.5 °C (Tveito, 2021). The warmest areas are found in
135 lower-lying areas in southern Norway, and particularly along the coast in the southwest, while the coldest areas are in the high
136 mountains and inland areas of the north. Norway also exhibits large spatial variability in precipitation, ranging from 212 mm
137 in southern parts of Northern Norway to 6130 mm close to the Ålfotbreen glacier in Western Norway. The wet areas along the
138 west coast are exposed to migrating low pressure systems most often arriving from the west-southwest (Lutz et al., 2024).

139 We selected 85 and 38 catchments for calibration and validation of the hydrological model, respectively. All these catchments
140 are near-natural catchments and 112 of the 123 catchments are smaller than 1000 km². The distribution of the catchments
141 represents various climate and hydrological regimes, geographic conditions and landscape types in Norway. The catchment
142 boundary is delineated by NVE and the gauges at the outlet of these catchments are shown in Fig. 1.



143

144 **Figure 1: the climatic and topographic characteristics of the simulation domain as well as the locations of glaciers and hydrological**
 145 **gauging stations and catchment boundaries.**

146 **2.2 Historical meteorological data**

147 The historical meteorological data is used as reference in the bias-adjustment procedures and for hydrological model calibration
148 and validations. It consists of nine atmospheric meteorological variables at a 1 x 1 km² grid covering Norway and river
149 catchments in neighbouring countries (Fig. 1): mean, minimum and maximum 2m temperature (K), precipitation flux (mm/s),
150 relative humidity (%), longwave and shortwave radiation (W/m²), pressure (Pa) and 10m wind speed (m/s).

151 Daily minimum, maximum and mean temperatures as well as precipitation are provided by the seNorge2018 v20.05 dataset
152 (Lussana et al., 2019; 2020). It covers the period 1957–2020 and is based on quality-assured daily datasets. The precipitation
153 values are adjusted for wind-induced under-catch based on Wolff et al. (2015). Note that seNorge2018 continuously
154 incorporates the latest available station data and is therefore not homogenized in time. This may affect the calculation of
155 changes within the historical period.

156 Daily wind speeds for Norway from 1958 to 2020 are obtained from the KliNoGrid 16.12 dataset. The KliNoGrid dataset is
157 based on the Norwegian atmospheric reanalysis NORA10 (Reistad et al., 2011) wind speed data, downscaled onto a 1 km grid
158 using a quantile mapping approach (Bremnes, 2004) to match the climatology of the high-resolution numerical weather
159 prediction model AROME-MEtCoOp (Müller et al., 2017).

160 Daily short- and longwave radiation, relative humidity and surface pressure are obtained from the HySN2018v2005ERA5
161 dataset. It is generated based on the ECMWF atmospheric reanalysis ERA5 (Hersbach et al., 2020) and seNorge2018 v20.05
162 and covers the period 1958–2020. The dataset is described in detail in Huang et al. (2022) and Erlandsen et al. (2021).

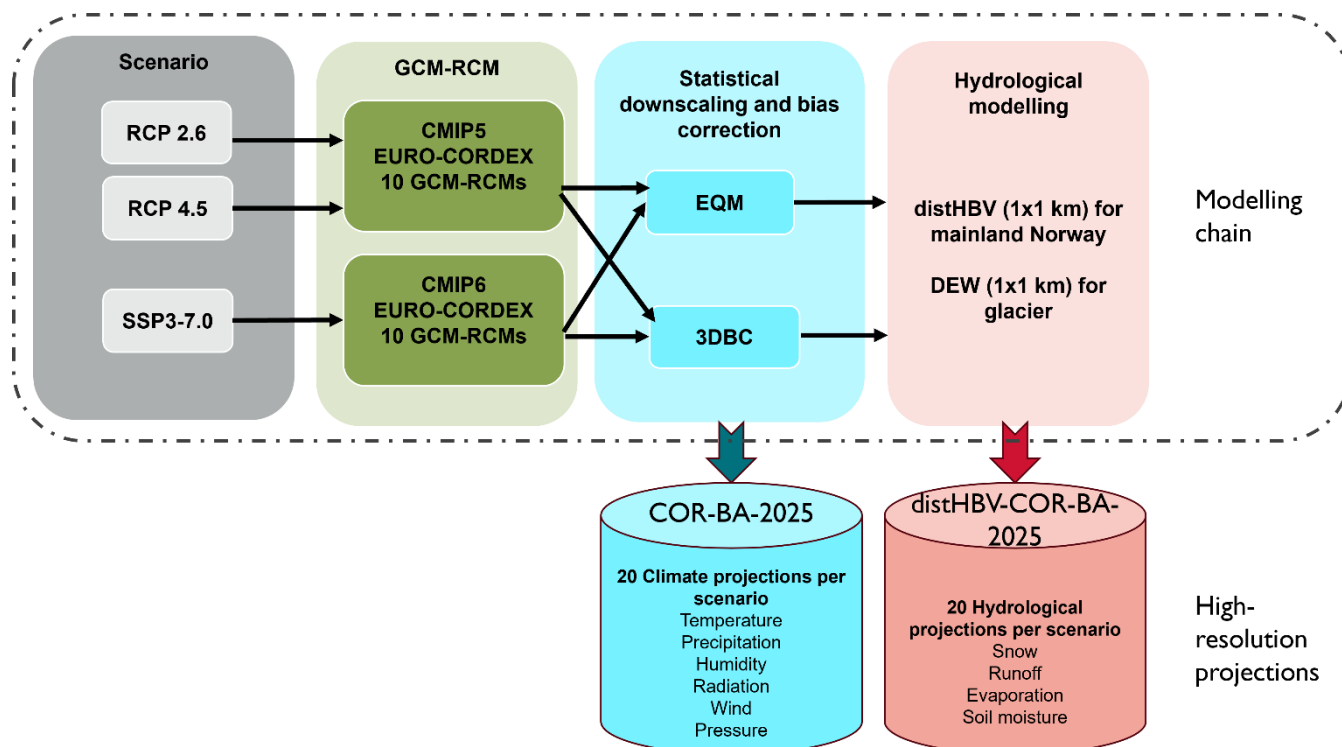
163 **2.3 Data for setting-up hydrological models**

164 To set up the hydrological model, a digital elevation model (DEM), as well as maps of soil type and land cover type with 1
165 km horizontal resolution are required. The DEM map was provided by the Norwegian Mapping Authority. Five soil types are
166 reclassified based on the sediment map from the Geological Survey of Norway (Erlandsen et al., 2021), and bare mountain
167 soil and moraine soils account for ca. 80% of the total mainland area. Nine land cover types (open area, bog, built-up, forest,
168 cropland, heather, bedrock, lake, permanent ice and snow) are classified based on the National Land Resource Map (Ahlstrøm
169 et al., 2014) and the remote sensing based forest resource map SAT-SKOG (Gjertsen and Nilsen, 2012). The forest land cover
170 is further classified into 12 structural forest types to distinguish three species groups (spruce, pine, and deciduous forest) and
171 four forest development stages (underdevelopment, two intermediate development stages and mature forest) (Majasalmi et al.,
172 2018). The parametrization for each forest structural type, such as maximum leaf area index, vegetation height and shortwave
173 albedo, is given by Majasalmi et al. (2018) and Bright et al. (2018). For glacier areas, the glacier modelling doesn't account
174 for variation of soil types and uses simplified land cover types including open area, bog, forest, bedrock and glacier area
175 coverage. However, it requires glacier ice thickness and glacier area data (Andreassen et al. 2015) to setup the model.

176 Discharge measurements from 123 gauging stations are used to calibrate and validate the hydrological model (Fig. 1). They
177 are quality-assured by NVE. All 123 stations have measured daily discharge from 1980 to 2014 with less than 5% missing
178 data. For the glacier modelling, mass balance data is only available for six glaciers and discharge measurements from 19
179 gauging stations downstream of the glaciers are used to calibrate and validate the hydrological model. All discharge and mass
180 balance data are publicly available at sildre.nve.no and glacier.nve.no/glacier/viewer/ci/en/.

181 **3 Modelling chain**

182 We followed the commonly used modelling chain in hydrological climate impact studies, i.e., 1) emission scenarios, 2) GCMs
183 and RCMs, 3) statistical downscaling and bias correction and 4) hydrological model (Fig. 2). The first component of the
184 modelling chain is to select emission scenarios. For the CiN-2025 report, two RCPs used in CMIP5 were selected, representing
185 a very stringent pathway (RCP2.6) and a moderate-emissions pathway (RCP4.5). The shared socioeconomic pathway SSP3-
186 7.0 used in CMIP6 was selected to represent the high-emission scenario. The reason why only one SSP scenario was selected
187 is that SSP1-2.6 and SSP3-7.0 were the first-priority scenarios for the EURO-CORDEX community (Katragkou et al., 2024).
188 The data has become available late with regard to the time needed to run our complete modelling chain - it is in fact still not
189 openly available - making the selection of more than one SSP scenario infeasible. Such a combination of CMIP5 and CMIP6
190 scenarios has also been used in other national climate projections, e.g., the climate projections in Switzerland published at the
191 end of 2025 (Schumacher et al., 2024) which combined EURO-CORDEX RCP8.5 with CMIP6 SSP5-8.5 GCM simulations.



192

193

Figure 2: Modelling chain to generate high-resolution climate and hydrological projections for the CiN-2025 report.

194

In the second component of the modelling chain the task is to select a representative model ensemble from the EURO-CORDEX simulations (Jacob et al., 2014) for each emission scenario. Within the EURO-CORDEX framework, CMIP5 and CMIP6 GCMs are downscaled by different RCMs, resulting in a set of GCM-RCM combinations. For CiN-2025 a larger EURO-CORDEX ensemble for RCP scenarios was available compared to CiN-2015, enabling a more robust data basis and requiring new model selection strategies (Section 4).

199

Once the model ensemble was identified, the next step was to downscale the RCM projections of atmospheric variables from the original grid size of approximately 12.5 km to 1 km. It was followed by removal of biases in RCM simulations relative to observed meteorological data (Section 2.2) in the calibration period. For future projections, we adjusted the values based on the corrections established in the calibration period under the assumption that the relationship between the observed and modelled data remains unchanged. Two bias-adjustment methods were used: de-trended empirical quantile mapping (denoted as EQM hereafter for simplicity) and three-dimensional bias-correction (3DBC) additionally to EQM (Section 5). The former is a widely used univariate bias-adjustment method and was used for CiN-2015. The latter adds a post-processing procedure, taking into account inter-variable dependencies. To our knowledge, this is the first time the 3DBC method is applied in Norway, and we have identified several strengths and weaknesses with this multivariate method (Section 5.3). Since the two bias-adjustment methods complement each other, we decided to apply both bias-adjustment methods on the RCM projections

208

209 and provided two complete datasets (EQM only and EQM with 3DBC). To assess the uncertainty in the climate and
210 hydrological projections from the choice of methods, we have carried out an uncertainty analysis (Section 7.3 and 8.3).

211 The last component of the modelling chain is hydrological modelling. The distHBV model was still the main tool for simulating
212 hydrological components under different climate scenarios for the CiN-2025 report, but two major improvements have been
213 made since CiN-2015. The first improvement was to replace the temperature-based evaporation method with the Penman-
214 Monteith equation in the distHBV model (Huang et al., 2019), because physical-based approaches, such as the Penman-
215 Monteith method, consider more climatic variables and provide more robust changes in potential evaporation under climate
216 scenarios than the empirical ones (McAfee, 2013; Tam et al., 2024). The second improvement was the use of Distributed
217 Element Water balance model (DEW) (Beldring, 2008) for glacierized regions. Since distHBV was not able to simulate the
218 changes in glacier area, glacier melt water can be unrealistically simulated under climate scenarios. In contrast, DEW is able
219 to simulate glacier area, volume and surface elevation dynamically and thus gives more reliable hydrological projections under
220 climate change for glacierized regions. Both models ran independently at 1 km spatial resolution and with daily time steps, but
221 distHBV ran for all grid cells in Norway and DEW only ran for the grid cells covering glacierized regions. A postprocessing
222 procedure was carried out to combine the distHBV and DEW outputs to generate final runoff projections for mainland Norway.

223 The modelling chain resulted in two datasets with a spatial resolution of 1x1 km at daily time steps, which will be serving as
224 the basis for climate impact assessment in mainland Norway. The first dataset is termed COR-BA-2025 (short for CORDEX-
225 Bias Adjusted, updated in 2025), consisting of 20 bias-adjusted high-resolution climate projections for each emission scenario
226 and is available from 1970 to 2100 (2098 depending on GCMs). These projections include nine atmospheric variables at 1x1
227 km spatial resolution and with daily time steps, each bias-adjusted both with EQM and 3DBC: mean, minimum and maximum
228 2m temperature (K), precipitation flux (mm/s), relative humidity (%), longwave and shortwave radiation (W/m²), surface air
229 pressure (Pa) and 10m wind speed (m/s). The second dataset is called distHBV-COR-BA-2025 and consists of 20 hydrological
230 projections for each emission scenario at the same spatial and temporal resolution and coverage as the atmospheric projections.
231 The hydrological projections include two flux variables (runoff and evaporation) representing average values over each grid
232 cell in mm/day, and two state variables (soil moisture and snow water equivalent), which describe the average condition of the
233 hydrological components in a grid cell with unit mm. The evaporation, soil moisture and snow water equivalent projections
234 were generated by distHBV, whereas the runoff projections were obtained by superimposing the results of the glacierized grid
235 cells from the DEW model on the runoff projections from distHBV.

236 To select the climate ensembles and assess future changes in climate and hydrology, we defined one reference period (1991–
237 2020) and two future periods (2041–2070 and 2071–2100). The reference period was selected by two factors: 1) a recent
238 climate period better represents today’s climate, and 2) 1991–2020 is the current standard normal period defined by the World
239 Meteorological Organization (WMO). However, in CMIP5 and CMIP6, the historical simulation runs end in 2005 and 2014,

240 respectively. Data from the emission scenario RCP4.5 was used to extend the historical period beyond 2005 for RCPs and the
 241 data from the emission scenario SSP3-7.0 was used to extend the historical period beyond 2014 for SSPs.

242 Since the main focus of this paper is on the description of the methods in the modelling chain rather than assessing climate
 243 and hydrological projections under different emission scenarios, we mainly present the methods and results for the RCP4.5
 244 scenario as examples in the following sections. However, the methods described in this paper are valid for all three scenarios.

245 **4 Selection of GCM–RCM combinations**

246 Currently, the EURO-CORDEX CMIP5 projections comprise the largest high-resolution regional climate model ensemble for
 247 Europe and Norway with more than 30 simulations based on RCP2.6, more than 20 simulations based on RCP4.5 and more
 248 than 70 simulations based on RCP8.5. However, there are (only) 17 model combinations covering all three RCPs (Table 1).
 249 To be able to do a proper comparison between future projections of different RCPs, it is important to use identical model
 250 combinations for each RCP. These identical model combinations comprise five GCMs, namely CNRM_CM5, EC_EARTH,
 251 HadGEM2-ES, MPI-ESM-LR and NorESM1-M. Given time and computational constraints, we defined an upper limit of ten
 252 model combinations that are used as forcing data for the hydrological models, thus seven model combinations had to be
 253 excluded.

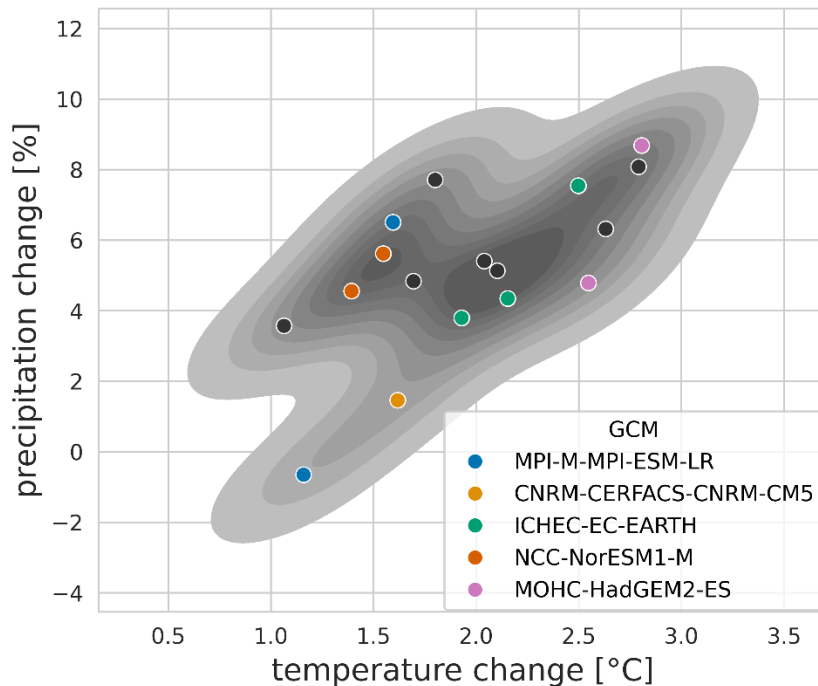
254 **Table 1. Summary of the 17 GCM-RCM combinations available for RCP2.6, RCP4.5 and RCP8.5. Combinations in bold were**
 255 **selected for downscaling and bias-adjustment for the mainland of Norway.** ¹: Original data has 360 days only. Additional days added.
 256 ²: Leap-year days added. ³: Spatial smoothing applied to tasmin, tasmax, tas and hurs.

Model combination name	GCM institute	modelling	GCM	RCM institute	modelling	RCM	Data coverage
cnrm-r1i1p1-aladin	CNRM-CERFACS		CNRM-CM5	CNRM		ALADIN63	1951–2100
ecearth-r12i1p1-rca³	ICHEC		EC-EARTH	SMHI		RCA4	1970–2100
ecearth-r12i1p1-cclm	ICHEC		EC-EARTH	BTU & KIT (CLMcom)		CCLM4-8-17	1950–2100
ecearth-r3i1p1-hirham³	ICHEC		EC-EARTH	DMI		HIRHAM5	1951–2100
hadgem-r1i1p1-rca^{1,3}	MOHC		HadGEM2-ES	SMHI		RCA4	1970–2098

hadgem-r1i1p1-remo¹	MOHC	HadGEM2-ES	GERICS	REMO2015	1950–2098
mpi-r1i1p1-cclm	MPI-M	MPI-ESM-LR	BTU (CLMcom)	CCLM4-8-17	1950–2100
mpi-r2i1p1-remo	MPI-M	MPI-ESM-LR	MPI-CSC	REMO2009	1951–2100
noresm-r1i1p1-rca^{2,3}	NCC	NorESM1-M	SMHI	RCA4	1970–2100
noresm-r1i1p1-remo	NCC	NorESM1-M	GERICS	REMO2015	1950–2100
cnrm_r1i1p1_alaro	CNRM-CERFACS	CNRM-CM5	RMIB-UGent	ALARO-0	1950–2100
cnrm_r1i1p1_racmo	CNRM-CERFACS	CNRM-CM5	KNMI	RACMO22E	1950–2100
ecearth-r12i1p1_racmo	ICHEC	EC-EARTH	KNMI	RACMO22E	1950–2100
ecearth_r12i1p1_remo	ICHEC	EC-EARTH	GERICS	REMO2015	1950–2100
hadgem_r1i1p1_racmo ¹	MOHC	HadGEM2-ES	KNMI	RACMO22E	1950–2098
hadgem_r1i1p1_hirham ¹	MOHC	HadGEM2-ES	DMI	HIRHAM5	1951–2098
mpi_r1i1p1_remo	MPI-M	MPI-ESM-LR	MPI-CSC	REMO2009	1951–2100

257

258 As a first quality check we used Table 6 in McSweeney et al. (2015) to see if the five GCMs perform satisfactorily in the
259 representation of two out of the three physical phenomena consisting of i) annual temperature and precipitation cycles, ii)
260 circulation and iii) storm tracks. This criterion did not lead to any exclusion of the 17 model combinations. As a next check
261 we verify if the GCM-RCM combinations are ranked in the ‘best half’ for 24 variables and impact-based indices (Table 2 in
262 Vautard et al., 2021) for the region of Scandinavia (Figure 12a in Vautard et al., 2021). This made us exclude cnrm
263 _r1i1p1_alaro. Further, we excluded three simulations performed with the RCM RACMO22E which are affected by a bug in
264 the snow albedo which again strongly affects the temperature signal above and around glaciers. This bug is documented in the
265 [EURO-CORDEX Errata table](#). Lastly, we checked the GCM-RCMs’ performance with respect to the observed temperature
266 and precipitation climate in Norway by using the seNorge v20.05 dataset as reference data. The differences between the
267 temperature biases in the remaining model combinations were found negligible. The largest precipitation biases (> 14 %) were
268 found for the historical simulations with hadgem2_r1i1p1_hirham, mpi-r1i1p1_remo and ecearth-r12i1p1_remo, hence we
269 excluded these simulations.



270

271

272

273

274

Figure 3. Projected changes in temperature and precipitation for mainland Norway by the end of the century relative to the reference period (1991–2020) under the RCP4.5 scenario (all dots). The grey shaded area indicates the distribution (kernel density estimate) of the projected changes comprising all 17 GCM-RCM combinations that were considered. The individual coloured points highlight the ten simulations selected for CiN-2025 (Table 1).

275

276

277

278

This leaves us with ten selected model combinations presented in Table 1. The projected changes in temperature and precipitation are shown for each model combination in Fig. 3. Based on the selected ten GCM-RCM combinations (coloured dots in Fig. 3), the projected changes in temperature and precipitation in Norway range from 1.2 °C to 2.8 °C and from -1 % to 9 % in the future period 2071–2100 relative to the reference period 1991–2020.

279

280

281

282

283

284

285

286

287

The selected GCM-RCM combinations vary in data coverage and quality (Table 1). The GCM HadGEM2-ES lacks 13 months towards the end of the time series, so we only used the simulations forced by this GCM until the end of 2098. When looking at near (2041–2070) and far future (2071–2100) changes, the HadGEM2-ES simulations were shifted by two years, i.e. the periods for HadGEM2-ES were 2039–2068 and 2069–2098. In addition, HadGEM2-ES driven EURO-CORDEX CMIP5 simulations use the HadGEM2-ES calendar with 360 days instead of 365 (366) days. To fill in the missing five days, we simply copied the day number 150, 210, 240, 300 and 360 from the 360-day year and added these extra days to the day number 151, 212, 243, 304 and 365 in a normal year. For a leap year, a copy of day number 59 was added similarly. This simple technique was also used on NorESM1-M coupled with RCA4 as this model combination does not support leap years. Unrealistically large snow accumulation at isolated grid cells have been discovered in the simulations from RCA4 and HIRHAM5. They were

288 considered as minor quality issues and their effects were reduced by applying a spatial smoothing on the variables minimum,
289 mean and maximum temperature, and humidity, an approach adopted from CH2018 (2018).

290 The selection criteria for the EURO-CORDEX CMIP6 projections are different from the ones for the EURO-CORDEX CMIP5
291 projections, because there were (only) 14 RCM simulations based on CMIP6 available by June 2024 (Table S1 in
292 Supplementary material). Also, a selection of CMIP6 GCMs providing a satisfactory performance over Europe and covering
293 a reasonable part of the climate change signal had already been carried out for the EURO-CORDEX CMIP6 simulations by
294 Sobolowski et al. (2025). The main criteria for the selection here were thus to include as many GCMs as possible, a balanced
295 RCM selection and excluding model combinations that show fairly similar results in temperature and precipitation over
296 Norway. This led us to exclude the model combinations ecearthveg_rli1p1fl_icon, ecearthveg_rli1p1fl_racmo and
297 miroc_rli1p1fl_hclim. We further excluded noresm_rli1p1fl_racmo due to a low climate sensitivity and small precipitation
298 changes during the summer months.

299 **5 Downscaling and bias-adjustment methods**

300 For CiN-2015, only daily mean temperature and precipitation were bias-adjusted, but for CiN-2025, nine surface variables
301 from the RCM outputs were downscaled and bias-adjusted, namely mean, minimum and maximum air temperature at two
302 meters height, precipitation, mean wind speed at 10 meters height, long- and shortwave radiation, surface pressure, and relative
303 humidity at two meters height.

304 The nine climate variables from the RCM outputs were firstly re-gridded to the seNorge grid with a 1 km spatial resolution
305 using the nearest-neighbour method. This conservative way to downscale from a coarse to fine scale grid ensures that the
306 original model outputs are preserved and not altered unintentionally by the downscaling step. The bias-adjustment procedure
307 was then implemented on the grid cell basis. Depending on the variable adjusted, different reference datasets (see Section 2.2)
308 were used for training.

309 Since the grid cells are bias-adjusted individually, we need to select methods that are computational efficient, or at least
310 applicable, and numerically stable (François et al., 2020) for a large number of grid cells (354 448 in total). We have tested a
311 few bias-adjustment techniques categorized as quantile mapping (Cannon et al., 2015) and multivariate approaches (François
312 et al., 2020). In the end, the univariate bias-adjustment adopting de-trended empirical quantile mapping (EQM) approach
313 (Bürger et al., 2013) was used to bias-adjust one climate variable at a time because the method meets all the aforementioned
314 criteria and is widely used in adjusting climate model data. EQM is effective in removing the model biases, preserving the
315 trend and climate change signal moments (i.e. mean and standard deviation) and estimating extremes. As no univariate method
316 can correct the possible biases in correlation among the atmospheric variables, all the EQM results were further post-processed

317 with the multivariate 3DBC approach (Mehrotra and Sharma, 2019) to rectify inter-variable, temporal and spatial dependency
318 structures.

319 **5.1 EQM**

320 The EQM approach adopted in this study is a de-trended variant of quantile mapping method which first establishes a statistical
321 transfer function for a variable between RCM outputs and reference data in the training period 1985–2014. Twelve calendar-
322 month-specific transfer functions were derived by fitting the empirical cumulative distribution functions (eCDFs) of the
323 modelled values with the eCDFs based on reference data for each grid cell. With these monthly bias-adjustments we correct
324 model biases which are varying throughout the year. This is essential for instance to produce realistic seasonal flow patterns
325 and hydrological regimes in the subsequent hydrological modelling. To avoid overfitting, daily data within a 3-month window
326 centred on the month of interest were pooled and used to develop the monthly eCDFs (Cannon et al., 2015). For example, data
327 from February to April were used to develop the eCDF for March.

328 The transfer functions were approximated by a series of empirical quantiles with fixed intervals of 0.01 spanning the probability
329 space (0,1) (Gudmundsson et al., 2012). Only the 1st to 99th quantiles were obtained and used. Linear interpolation was applied
330 for values in between those fixed quantiles. For values smaller than the 1st quantile and larger than the 99th quantile, linear
331 extrapolation was performed based on the slopes derived from the 1st and 2nd quantiles and 98th and 99th quantiles
332 respectively. These functions are assumed to be applicable to the projection period.

333 Wet-day correction has also been applied prior to bias-adjustment of precipitation. In our study region, RCMs generally provide
334 more rainy days than observed ones (see e.g. Lhotka et al., 2024). Thus, for each grid cell, a threshold value is derived such
335 that the wet-day frequency in modelled precipitation is equal to that in the corresponding reference data for the training period.
336 All modelled precipitation values which are below the derived threshold value are then set to zero for both training and
337 projection periods (Gudmundsson et al., 2012).

338 To reduce the potential impact of over-adjustment (modifying the long-term linear trend) and extrapolation (model-projected
339 values lying outside the range of the historical distribution), the long-term linear trend (usually 30-year) of the projected period
340 was first removed from model projections. Scaling the range of future projection to align closer to the historical one improves
341 the applicability of the transfer function by reducing the need to extrapolate beyond historical values, while the daily variability
342 about the monthly mean remains unchanged. The trend was reimposed after the bias-adjustment of the residuals. For all the
343 variables other than temperatures, trend removal and reimposition were performed multiplicatively, i.e. variability and
344 residuals were considered as ratios rather than differences. The procedure was applied separately for twelve months. For
345 example, for precipitation for month i , the scaling factor δP_i , which also represents the relative precipitation trend, is defined
346 as:

$$347 \quad \delta P_i = \bar{P}_i^{prj} / \bar{P}_i^{tnq} \quad (1)$$

348 where \bar{P}_i^{prj} and \bar{P}_i^{tnq} refer to mean monthly accumulated precipitation for month i for the projection and training periods,
 349 respectively. The de-trended daily precipitation in the projection period for a specific calendar month i (=Jan., Feb., ..., Dec.),
 350 $\hat{P}_i^{prj}(t)$, is:

$$351 \quad \hat{P}_i^{prj}(t) = P_i^{prj}(t) / \delta P_i \quad (2)$$

352 where $t = 1, 2, \dots, N_i$ is the time step, and N_i the number of days belonging to the calendar month i in the projection period.
 353 $P_i^{prj}(t)$ denotes the original RCM daily precipitation time series for month i in the projection period. EQM was applied to the
 354 de-trended time series, and the precipitation trend for month i was then re-introduced to the bias-adjusted de-trended results
 355 $\check{P}_i^{prj}(t)$ for month i . The bias-adjusted precipitation, $\check{P}_i^{prj}(t)$, for month i can be obtained by:

$$356 \quad \check{P}_i^{prj}(t) = \hat{P}_i^{prj}(t) \cdot \delta P_i \quad (3)$$

357 Similarly linear trend removal and reimposition for the projected values of temperature variables were done additively.
 358 Following similar notation, the temperature trend, δT_i , for month i simply equals to $\bar{T}_i^{prj} - \bar{T}_i^{tnq}$, and the de-trended daily
 359 temperature, $\hat{T}_i^{prj}(t)$, can be derived from:

$$360 \quad \hat{T}_i^{prj}(t) = T_i^{prj}(t) - \delta T_i \quad (4)$$

361 where $T_i^{prj}(t)$ represents the original RCM daily temperature for month i in the projection period. The bias-adjusted
 362 temperature for month i , $\check{T}_i^{prj}(t)$, can be recovered by adding the temperature trend δT_i to the bias-adjusted de-trended data
 363 $\hat{T}_i^{prj}(t)$:

$$364 \quad \check{T}_i^{prj}(t) = \hat{T}_i^{prj}(t) + \delta T_i \quad (5)$$

365 The projection period starting from 2015 to 2100 was further divided into seven overlapping 30-year time slices. The first time
 366 slice, however, only covers 2015-2040, followed by 2021-2050, 2031-2060, etc. After the bias-adjustment of each time slice
 367 using the established monthly transfer functions, only the 10-year results in the middle of the period were being kept. This
 368 procedure can better preserve the decadal trend but at the same time might introduce discontinuities in the time series at the
 369 start of each decadal period. The impact of such jumps in e.g. temperature might affect the snow accumulation in hydrological
 370 modelling at the transitions between the decadal periods. On the other hand, such jumps are negligible when the focus is on
 371 overall 30-year statistics. The impact of this approach is also expected to be smaller than shifting the entire 30-year window
 372 in each iteration. This is a pragmatic way to handle a basic limitation of the method. For the first and the last time slices, the
 373 results of the first 16 years and the last 20 years were used respectively. A continuous time series covering the whole projection
 374 period was put together afterwards.

375 5.2 3DBC

376 The bias-adjusted climate projections based on the univariate EQM approach show the same dependency structures as the
377 uncorrected RCM simulations. To impose inter-variable, temporal and spatial dependency structures obtained from the
378 reference datasets, an additional post-processing step has been applied. The multivariate method we used for this is called
379 3DBC (three-dimensional bias-correction) as it adjusts along the three dimensions: variables, time and space. It is described
380 in detail in Mehrotra and Sharma (2019). 3DBC is re-establishing the spatial, temporal and inter-variable structures from the
381 reference data by reordering the daily EQM values according to observed time-ranks at each grid-point, resulting in the bias-
382 adjusted data having the same rank structure (ordering) as the reference data in the calibration period. Compared to other
383 multivariate bias correction methods (e.g. the MBCn method developed by Cannon, 2018) the computational requirements of
384 3DBC are relatively small, making its application on a large number of grid cells feasible. Note that 3DBC adjusts the ranks
385 for future periods according to changes in the temporal auto-correlations as simulated by the RCMs. Thus, it does not strictly
386 assume that the dependency structures remain stable in future climates. However, while the original implementation by
387 Mehrotra and Sharma (2019) works on single calendar days across a future period of 30 years, our future period (2021-2100)
388 consists of 80 years. Following the original approach would have resulted in imposing observed trends repeatedly on the future
389 period. We thus adapted the 3DBC method to work within single years of the EQM data, an approach that maintains the climate
390 change signals and trends from the RCMs (and EQM) on an annual scale. As a result, the adjustments in the variable auto-
391 correlations for the future periods have a limited effect and do not fully transfer the dependency structure changes from the
392 RCMs to the 3DBC bias-adjusted data. Since 3DBC reshuffles the bias-adjusted times series resulting from EQM within a
393 year, the marginal distributions at seasonal scale might be modified.

394 5.3 Evaluation of bias-adjustment methods

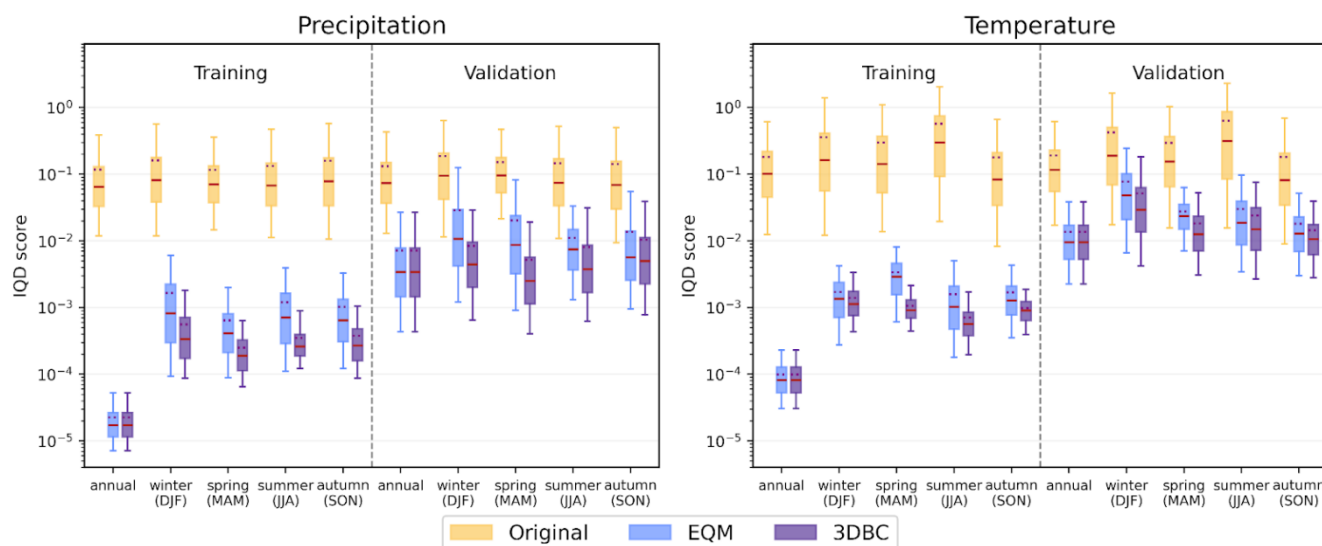
395 5.3.1 Performance of bias-adjustment methods

396 Thorarinsdottir et al. (2013) proposed the use of integrated quadratic distance (IQD) as a performance measure to compare the
397 full distribution of climate model output to the corresponding distribution of observed data. IQD was further employed by
398 Yuan et al. (2019; 2021) to assess the performance of different bias-adjustment approaches. IQD (Eq. 6) is defined as:

$$399 d_{IQ}(F, G) = \int_{-\infty}^{+\infty} (F(t) - G(t))^2 dt \quad (6)$$

400 where F , G are two cumulative distribution functions. $d_{IQ}(F, G)$ summarizes the differences, and a lower value implies a
401 smaller difference between F and G . $d_{IQ}(F, G) = 0$ if $F = G$. For further details, please see Thorarinsdottir et al. (2013). In this
402 study, we compared the eCDFs of bias-adjusted precipitation and temperature with corresponding seNorge2018 v20.05 data
403 over the training (1985–2014) and validation (1960–1984 or 1970–1984 depending on the period start of the RCM) periods
404 in each grid cell. In addition, we calculated IQD scores derived from comparison of original RCM outputs with the observed
405 data.

406 IQD scores for precipitation and temperature are presented in Fig. 4. The results clearly demonstrate that both bias-adjustment
 407 approaches are far better at reproducing the full distributions of observed precipitation and temperature by several orders of
 408 magnitude than the original RCM outputs. As expected, the improvements are larger (smaller d_{IQ}) in the training period than
 409 the validation period. EQM and 3DBC have the same performance on annual results, but 3DBC generally performs better than
 410 EQM on seasonal results because 3DBC utilizes additional information about the intra-annual order of the observed time series
 411 in the post-processing. The only exceptions are the IQD scores from particular RCMs (CCLM4-8-17, REMO2015 and
 412 REMO2009), which show that EQM provides marginally better results than 3DBC in autumn (Fig. S1 in Supplementary
 413 materials). It might indicate that the observed ranks in autumn of the training and validation periods are quite different and
 414 that those models partly capture this change. Overall, 3DBC provides added value as compared to EQM when seasonal
 415 statistical properties are of importance.

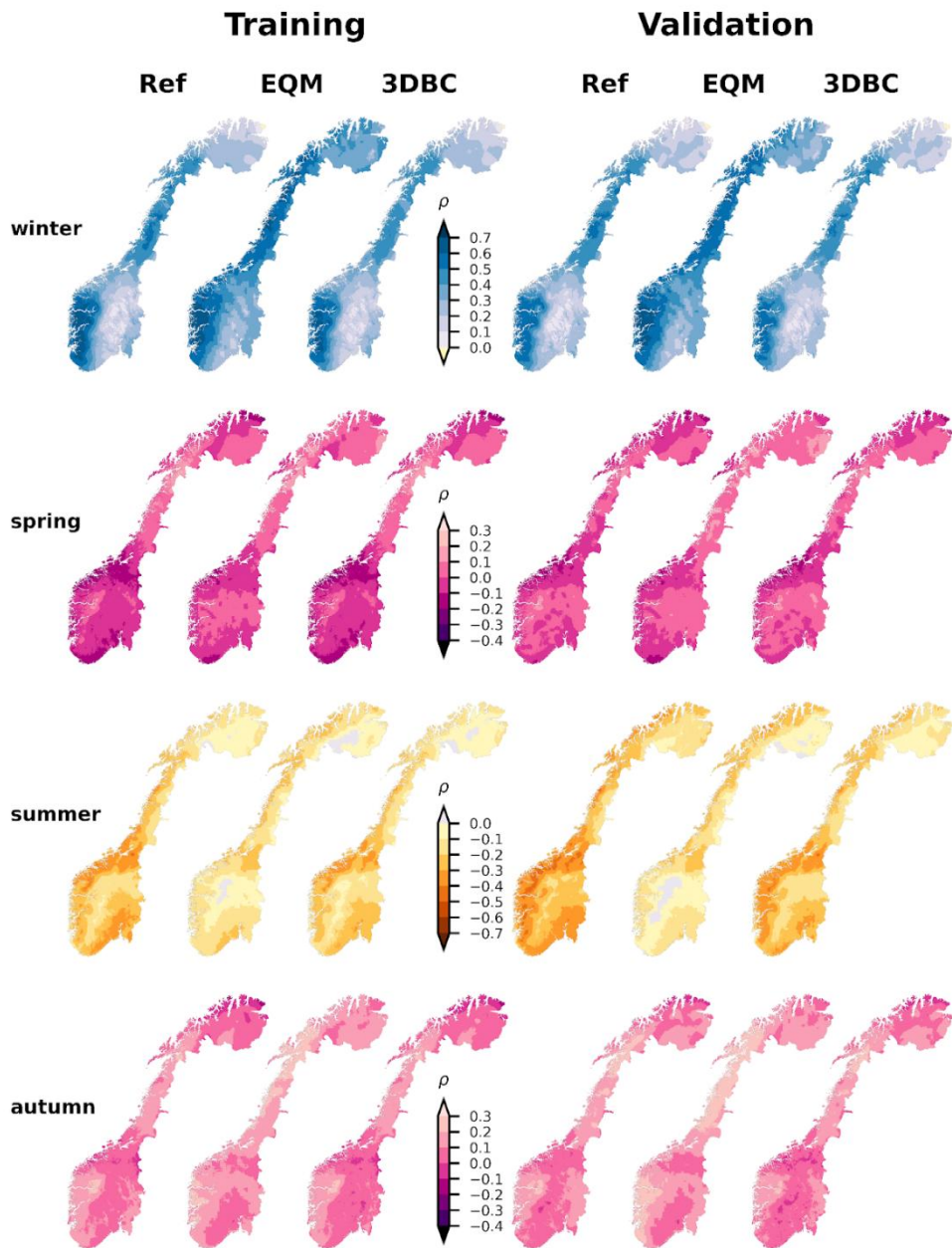


416

417 **Figure 4: Integrated quadratic distance (IQD) scores for precipitation (left panel) and temperature (right panel) based**
 418 **on the CMIP5 model ensemble. Bias-adjusted results from EQM and 3DBC in addition to the original model outputs**
 419 **are compared with the reference datasets seNorge2018 v20.05 over the training (1985–2014) and validation (1960/70–**
 420 **1984) periods. The red line on the box indicates the median value whilst the dotted line represents the mean. The lower**
 421 **and upper boundaries of the box are the 25th and 75th percentiles. The lower and upper ends of the whiskers refer to**
 422 **the 5th and 95th percentiles.**

423 Besides the seasonal statistics, 3DBC can simulate better spatial correlation structures between precipitation and temperature
 424 in the historical period than EQM, as it reorders the modelled ranks of precipitation and temperature based on observations
 425 while the univariate EQM method keeps the spatial rank correlation pattern from the RCM. Figure 5 shows an example of the

426 spatial distribution of seasonal Spearman's rank correlation coefficient (ρ), calculated based on the bias-adjusted datasets from
427 EQM and 3DBC and the reference datasets for training (1985–2014) and validation (1960–1984) periods for one RCM. In
428 general, ρ are largest and positive in winter (warm days are wetter), followed by negative ρ in summer (warm days are dry,
429 cold are wet). In spring and autumn, ρ is much smaller than in summer and winter, indicating a rather weak rank correlation
430 between precipitation and temperature. The differences in the spatial correlation structure between these two methods are often
431 most pronounced in winter and summer. EQM usually overestimates the positive rank correlations almost over the whole
432 country in winter, whilst it underestimates negative dependencies in summer. And this spatial rank correlation pattern seems
433 to be rather stable from one period to another. Aggregated results for each model combination are shown as boxplots (Fig. S2
434 in Supplementary materials), and they confirm that 3DBC performs better in recovering the inter-variable spatial dependency
435 structure for all RCMs.

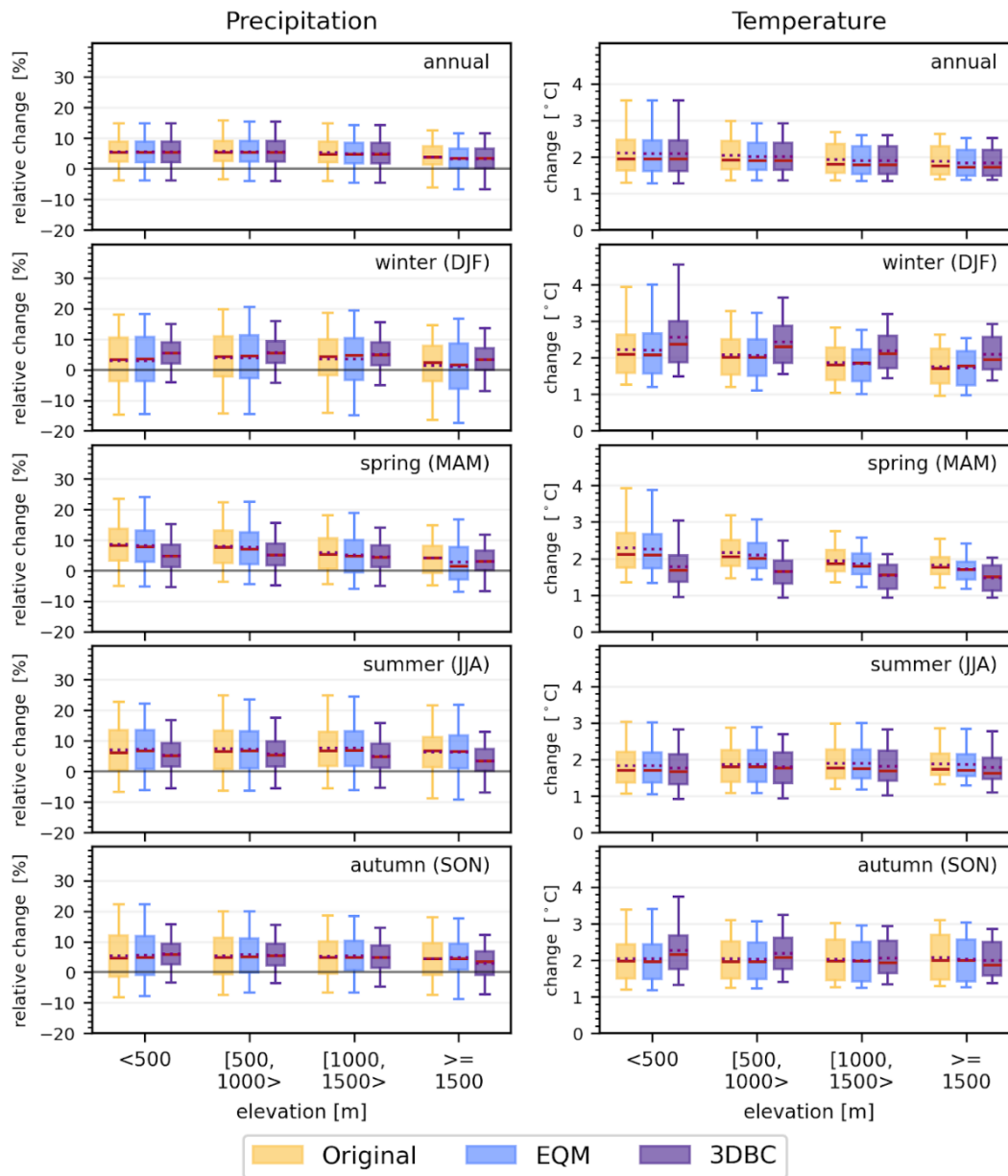


436

437 **Figure 5: Spatial distribution of Spearman's rank correlation coefficient ρ of daily precipitation and temperature in winter (DJF),**
 438 **spring (MAM), summer (JJA) and autumn (SON) for the two bias-adjustment methods. For training (1985–2014) and validation**
 439 **(1960–1984) periods, the two bias-adjusted datasets, EQM and 3DBC are based on historical run from CMIP5-based mpi-r11p1-**
 440 **cclm and compared with reference datasets seNorge2018 v20.05.**

441 **5.3.2 Climate change signal preservation**

442 The two bias-adjustment methods can lead to different climate change signals in the future periods (e.g. 2071-2100) relative
443 to the reference period (1991-2020). Figure 6 shows the annual and seasonal changes grouped in four elevation bands (< 500,
444 [500, 1000>, [1000,1500>, > 1500), including 52%, 32.7%, 13.6% and 1.7% of the grid cells in Norway, respectively. The
445 result aligns with other recent studies demonstrating that the change signals are elevation-dependent (Astagneau et al.,2025,
446 Matiu et al., 2024). The two bias-adjustment methods provide identical annual climate change signals, since 3DBC uses the
447 same bias-adjusted results from EQM before further post-processing. EQM generally preserves the seasonal climate change
448 signals from the original RCMs in terms of both mean and median changes as well as the spread of changes for all elevation
449 bands. However, by reshuffling the chronological order intra-annually, 3DBC modifies the seasonal change signals from the
450 original RCMs, leading to larger increases in precipitation and temperature in winter and smaller increases in spring than the
451 original RCM outputs. In summer and autumn, the climate change signals can be underestimated or overestimated by 3DBC
452 depending on the variables and elevations.



453

454 **Figure 6: Projected annual and seasonal changes in precipitation (relative change in %, left column) and temperature (change in**
 455 **°C, right column) from 1991–2020 to 2071–2100 for RCP4.5 in terms of elevation. Results grouped in four elevation bands from two**
 456 **bias-adjustment procedures, EQM and 3DBC, are compared to the original RCM projections. The red line on the box indicates the**
 457 **median value whilst the dotted line represents the mean. The lower and upper boundaries of the box are the 25th and 75th percentiles.**
 458 **The lower and upper ends of the whiskers refer to the 5th and 95th percentiles.**

459 **6 Hydrological modelling**

460 **6.1 distHBV**

461 distHBV is a spatially distributed version of the HBV precipitation-runoff model (Beldring et al., 2003) and is the major tool
462 applied to assess hydrological responses to climate change in Norway. The model calculates the water balance for 1 x 1 km
463 grid cells at a daily time step covering the entire mainland surface area of Norway and upstream areas in Finland and Sweden
464 contributing to streamflow in Norwegian catchments. Each grid cell includes one soil type and up to five land cover types.
465 distHBV has components for accumulation, sub-grid scale distribution and ablation of snow, interception storage, sub-grid
466 scale distribution of soil moisture storage, evapotranspiration, groundwater storage and runoff response, lake evaporation and
467 glacier mass balance. The newly implemented Penman-Monteith method and the prescribed parameterizations are presented
468 in Huang et al. (2019) and Erlandsen et al. (2021).

469 As for other conceptual hydrological models, calibration is necessary to adjust the distHBV parameters to improve the model
470 performance of reproducing observed discharge, due to the absence of directly measured catchment characteristics, natural
471 variability and the non-linearity of the processes involved. Since all parameters to calculate potential evaporation are prescribed
472 in the Penman-Monteith equation, the calibration parameters are mainly associated with lake, subsurface, snow and glacier
473 processes (Table 2). Different from the lumped version of HBV, the parameters associated with snow and subsurface processes
474 in distHBV vary by land cover type (deciduous forest, coniferous forest and others) and soil-type (the five soil types based on
475 the sediment map (Section 2.3) plus glacier bed), respectively. In total, there are 44 parameters for modelling mainland of
476 Norway, including six snow parameters (two snow parameters times three land use classes), 36 soil parameters (six soil types
477 times six subsurface parameters) and two parameters associated with lake and glacier processes. The parameters vary between
478 grid cells due to different combinations of soil and land cover types within grid cells. Note that we didn't distinguish the snow
479 parameters for all land cover types because it will increase equifinality risks due to too many calibration parameters and forest
480 is one of the dominant land cover types in Norway (Huang et al., 2026). In addition, we didn't correct rainfall or snow as in
481 other HBV applications, because it will lead to inconsistency between the climate and hydrological projections in terms of
482 water balance.

483 **Table 2: list of calibration parameters. Note that the parameters associated with the snow and subsurface processes vary by land**
484 **cover and soil type, respectively.**

485

Associated process	Parameter	Explanation	Unit	Min	Max
Lake	KLAKE	Rating curve constant	-	1.00E-04	0.1
Snow and glacier	SMELT_T	Snow melt temperature	°C	-1	2
	SMELTR	Temperature index for snow melt rate	m/°C	1.00E-04	0.01
	IMELTR	Ice melt rate for glaciers additional coefficient to SMELTR	-	1	4
Subsurface	FC	Field capacity	m	1.00E-02	1
	BETA	Shape coefficient of soil moisture	-	1	5
	KUZ	Upper zone recession coefficient	-	1.00E-03	1
	ALFA	Upper zone nonlinear drainage coefficient	-	1	2
	PERC	Percolation from upper zone to lower zone	-	1.00E-03	0.5
Subsurface	KLZ	Lower recession coefficient	-	1.00E-03	1

486

487 The model was calibrated against discharges at 85 gauges (Fig. 1) from 2000 to 2007 using the parameter estimation routine
488 PEST (Doherty and Skahill, 2006) and a multi-criteria calibration approach (Huang et al., 2019). The multi-criteria include the
489 Nash and Sutcliffe efficiency (NSE) (Nash and Sutcliffe, 1970), the bias in water balance (BIAS) and the volume bias in the
490 high-flow segment of the flow duration curve (ΔFHV , 0 – 0.02 flow exceedance probabilities) (Yilmaz et al., 2008). Since
491 PEST minimizes the difference between the criteria results and their ideal values (1 for NSE and 0 for biases), the calibration
492 objective function θ containing the three criteria at multiple gauges can be formulated as Eq. 7.

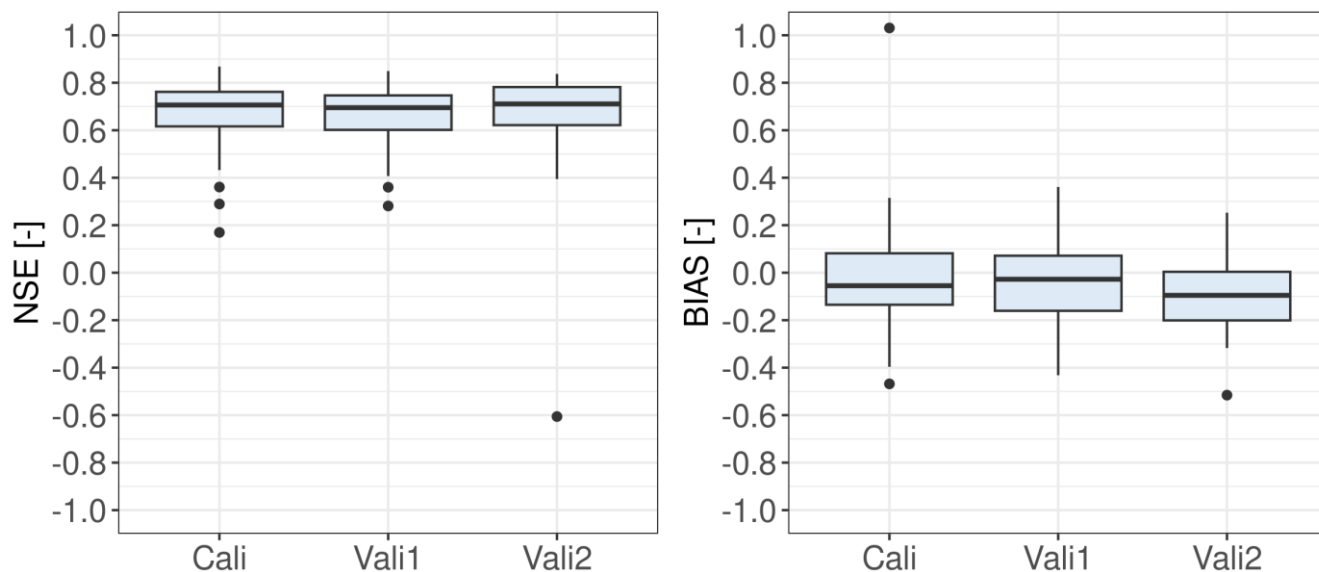
$$493 \theta = W_{NSE} * \sum_{i=1}^n (1 - NSE_i)^2 + W_{BIAS} * \sum_{i=1}^n (BIAS_i)^2 + W_{\Delta FHV} * \sum_{i=1}^n (\Delta FHV_i)^2 \quad (7)$$

494 where W are weights for each criterion and $n = 85$, the number of calibration catchments. W_{NSE} equals to 8 and W_{BIAS} and
495 $W_{\Delta FHV}$ equal to 1 to achieve a good calibration performance.

496 Five PEST runs were carried out with different initial parameter values and only the parameter set giving the best model
497 performance was selected for model validation. The model was validated against the discharge of the 85 calibration stations
498 and additional 38 gauging stations from 2011 to 2020 to evaluate the temporal and spatial transferability of the model,
499 respectively. The validation period (2011 – 2020) was selected because it is the warmest period for most catchments in the
500 recent decades. Compared to the calibration period (2000 – 2007), the average increase in annual mean temperature of all 123
501 catchments is about 0.43 degrees in 2011 – 2020. Hence, the validation results show the model performance under warmer
502 conditions.

503 Figure 7 shows the calibration and validation results in terms of NSE and BIAS. During the calibration period, about 50% and
504 29% of the catchments show good ($NSE > 0.65$ and $|BIAS| < 0.1$) and satisfactory ($0.65 > NSE > 0.55$ and $0.1 < |BIAS| < 0.15$) results
505 (Moriassi et al., 2007), respectively. The model generally underestimates discharge with the median bias of -5%, mainly due to
506 underestimation of precipitation in seNorge2018 v20.05 data. The model performs similarly in terms of NSE in the validation
507 period for the 85 gauging stations, with the median NSE degraded by only 0.01. The median bias is reduced by 0.025 in the
508 validation period than in the calibration period but there are more catchments with $|BIAS| > 0.1$. The model performance varies

509 with time, partly due to parameter transferability problems under different climate conditions and partly due to the quality of
 510 seNorge2018 v20.05 dataset that also varies with time (Lussana et al., 2019; 2020). The validation results for the additional
 511 38 gauging stations show robust spatial transferability of the model, with good or satisfactory ($NSE > 0.55$ and $|BIAS| < 0.15$)
 512 model performance for about 58% of the catchments. The model generally underestimates discharge with BIAS less than -0.1
 513 for about half of the validation gauging stations. Such calibration and validation results are acceptable with consideration of
 514 the quality of the meteorological forcing data in such a mountainous region and simultaneous calibration for all catchments.



515
 516 **Figure 7: distHBV model performance in terms of NSE and BIAS for the 85 calibration catchments in the calibration period 2000 –**
 517 **2007 (Cali), for the 85 calibration catchments in the validation period 2011 – 2020 (Vali1) and for the 38 validation catchments in**
 518 **the validation period 2011 – 2020 (Vali2).**

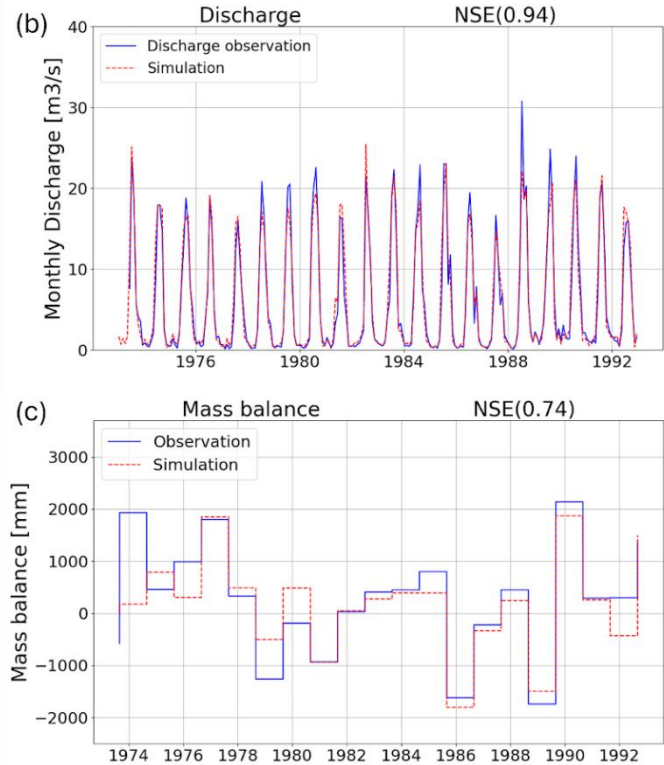
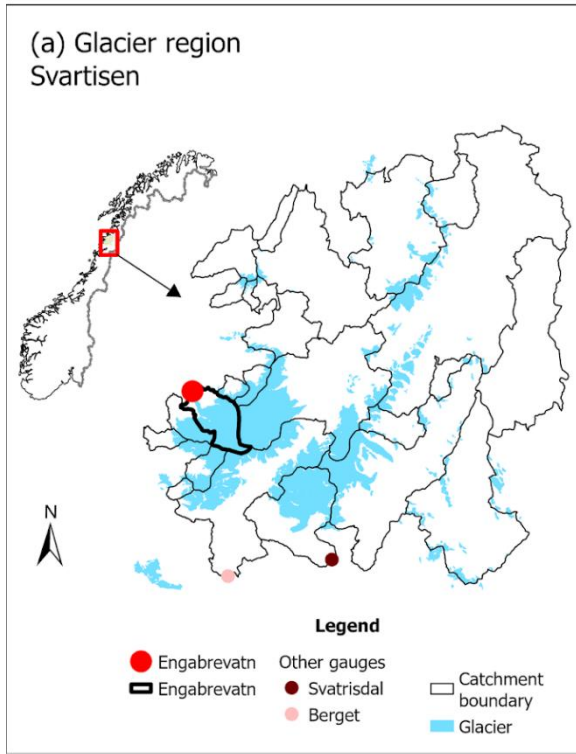
519 **6.2 DEW**

520 Distributed Element Water balance model (DEW) hydrological model (Beldring, 2008; Li et al., 2015) was used to simulate
 521 climate change impacts on glaciers for 12 given glacier regions in Norway. The smallest glaciers (< 1 km²) were omitted in
 522 the DEW model. This model differs from distHBV in the respect that it also calculates changes in glacier ice area, volume and
 523 surface elevation, and water balance. In addition, the model requires additional information as input, such as ice thickness and
 524 glacier area for grid cells with glaciers. However, DEW uses only daily mean temperature and precipitation as meteorological
 525 forcing data as it uses a temperature-based degree-day model to estimate potential evapotranspiration.

526 Snow and glacier ice melt were calculated using a degree-day model, with different degree-day factors for snow and ice. DEW
527 applies a simplified model called DeltaH (Huss et al., 2010) to describe the changes in glacier ice area, volume and surface
528 elevation. The method simulates the impacts of ice movement that transports mass from the highest to the lowest areas of the
529 glacier. Simulations without taking this redistribution of glacier ice into account will give incorrect estimates for both glacier
530 changes and the water flow from the glacier. It is based on historically observed elevation changes of the glacier surface
531 elevation and how these are distributed over the glacier area. The pattern of change is then used when simulating the
532 development of glacier ice area, volume and surface elevation under climate scenarios by having the model redistribute mass
533 over the glacier at the end of each mass balance year. Ice melt caused by negative mass balance results in diminishing of the
534 glacier ablation area. Simulations with more advanced, physically based glacier models that simulate the flow of ice in the
535 glaciers would probably be more realistic but are more demanding to run and require much more input data that are not
536 available for most glacier areas in Norway.

537 DEW was calibrated using the same parameter estimation routine (PEST) as used for distHBV, but it was calibrated against
538 observed daily streamflow and annual mass balance data for six out of the 12 glacier regions. Within each of the six regions,
539 one optimal model parameter set was determined for all glaciers and catchments. This strategy was chosen to avoid
540 discontinuities in model results between or along catchment boundaries and ice divides. Fixed periods were not used for
541 calibration and validation as in the case of distHBV, because the availability of observed data varied both in time and space.
542 It was a challenge to find both mass balance and streamflow time series of good quality at the same period, leading to limited
543 time series available for model validation in some cases. During model calibration, mean NSE value is 0.75 for daily discharge
544 of 19 gauging stations downstream of the glaciers, and 0.72 for annual mass balance for six glaciers. The mean NSE value for
545 daily discharge during model validation is 0.74. For the remaining six glacier regions where there were no streamflow data
546 available, model parameters were transferred from the nearest glacier region with calibrated parameters.

547 Figure 8a shows one of the 12 glacier regions, called Svartisen, as an example. For this region, DEW was setup for all
548 catchments where glacier melt contributes to river discharge. Among these catchments, only three catchments (Engabrevatn,
549 Svartisdal and Berget) have discharge observations in good quality and only Engabrevatn has the measured mass balance data.
550 Based on the data availability of both discharge and mass balance data, DEW was calibrated against the discharge of the three
551 catchments and glacier mass balance in Engabrevatn for the period 1974–1993. The calibrated parameters were then
552 transferred to other catchments of this region for hydrological projections. Figure 8b and 8c compare the observed and
553 simulated discharge and mass balance for Engabrevatn in the calibration period. It shows that the model can well reproduce
554 both monthly discharge and annual glacier mass balance with NSE larger than 0.7.



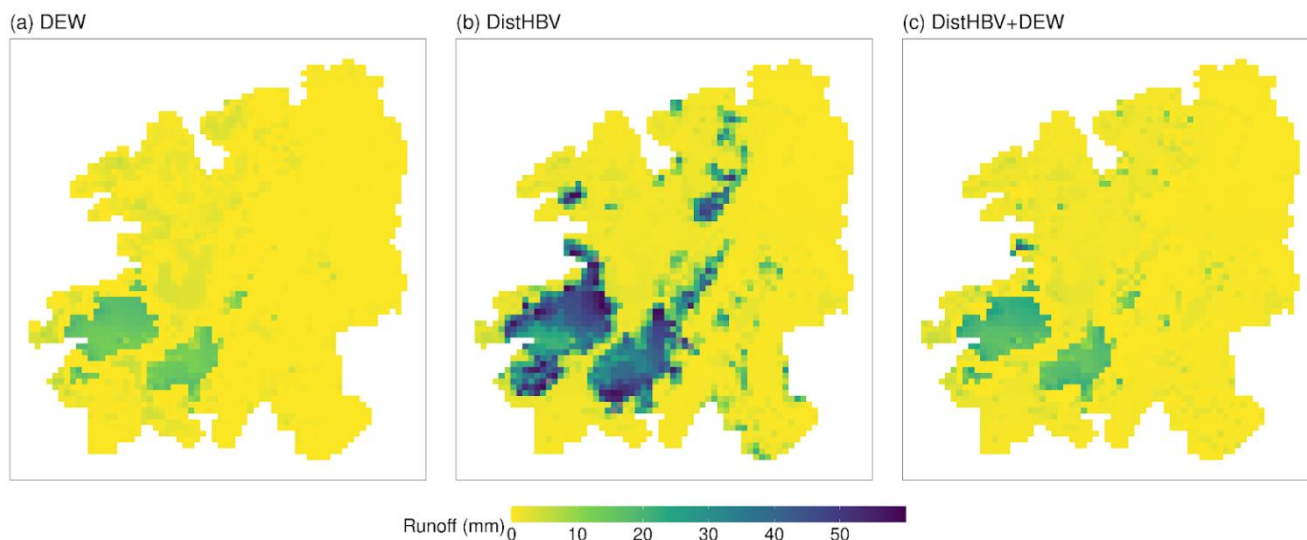
555

556 **Figure 8: The glacier region Svartisen (a), observed and simulated discharge (b) and annual mass balance (c) for the catchment**
557 **Engabrevatn.**

558 **6.3 Postprocessing of distHBV and DEW outputs**

559 The final runoff projections for mainland Norway were produced by replacing distHBV outputs with the DEW ones. Note that
560 DEW simulated the whole glacierized catchments but we only masked the glacierized grid cells in the historical period (e.g.,
561 the blue-color area within the catchments in Fig. 8a) for postprocessing. It is mainly because DEW uses a simpler potential
562 evapotranspiration (PET) method and rougher landuse/soil classes for non-glacierized area than distHBV. The mask of the
563 glacierized grid cells remained unchanged during the whole postprocessing procedure and the DEW outputs on the masked
564 grid cells replaced the distHBV ones at each time step in both historical and future periods. Figure 9 (a and b) shows the
565 simulated runoff projections using DEW and distHBV for the glacier region Svartisen (Fig. 8a) on 31st August 2100 driven by
566 the ecearth-r12i1p1-cclm climate projection. Without considering glacier retreat, distHBV projected high runoff (> 20 mm)
567 for most grid cells where glaciers exist in the historical period while DEW projected much lower runoff for these grid cells
568 than distHBV, confirming that distHBV overestimates runoff under warming conditions. After we replaced the distHBV results
569 with the DEW ones, the final output is more reasonable for this region than the distHBV one (Fig. 9c). Note that there are still

570 single grid cells with high runoff in the final product because of slightly different glacier maps used by DEW and distHBV. In
571 addition, small glaciers outside the glacierized catchments (Fig. 8a) were not simulated by the DEW model and the results for
572 these small glaciers cannot be corrected.



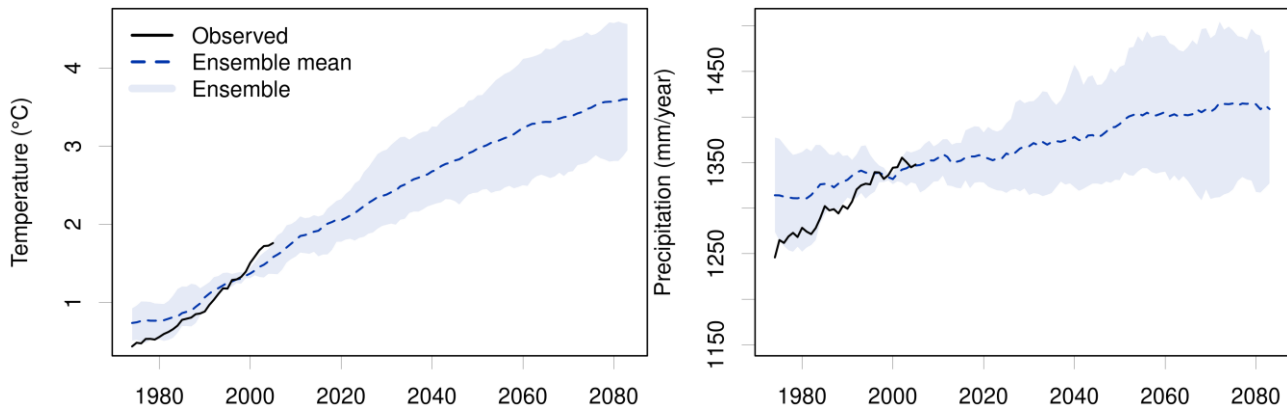
573

574 **Figure 9: Simulated runoff on 31st August 2100 for the glacier region Svartisen by DEW (a), distHBV (b) and the combination of**
575 **distHBV and DEW (c) driven by the ecearth-r12i1p1-cclm climate projection.**

576 7 National climate projections

577 7.1 Ensemble means and ranges

578 There are 20 climate projections for mainland Norway at 1km spatial resolution with daily time steps under the RCP4.5
579 scenario from the COR-BA-2025 dataset. Figure 10 shows 30-year running means of annual temperature and precipitation
580 sums from 1971 to 2098 for Norway. There is a clear increase in temperatures visible in the mean and the whole ensemble.
581 For precipitation, the ensemble mean is also increasing but the lower limit of the projection ensemble is showing a stable
582 precipitation amount of about 1325 mm/year. The observed historical values are mostly within the simulated precipitation and
583 temperature ensembles but are located at the lower end of the ensemble before the year 2000 and at the upper end afterwards,
584 indicating that the RCP4.5 ensemble underestimates recent temperature and precipitation trends in Norway. Note that all RCMs
585 are bias-adjusted to match the observed values averaged over the training-period 1985-2014 and the spread in the ensemble
586 equals zero for the middle of that period (year 2000). In addition, the ensemble spread is exactly the same for both EQM and
587 3DBC methods as 3DBC has the same change statistics as EQM on an annual basis.



588

589

590

Figure 10: Simulated 30-year running means of temperature (left) and precipitation (right) from the COR-BA-2025 ensemble of 20 climate projections (10 GCM-RCM combinations x 2 bias-adjustment methods) for Norway under the RCP4.5 emission scenario.

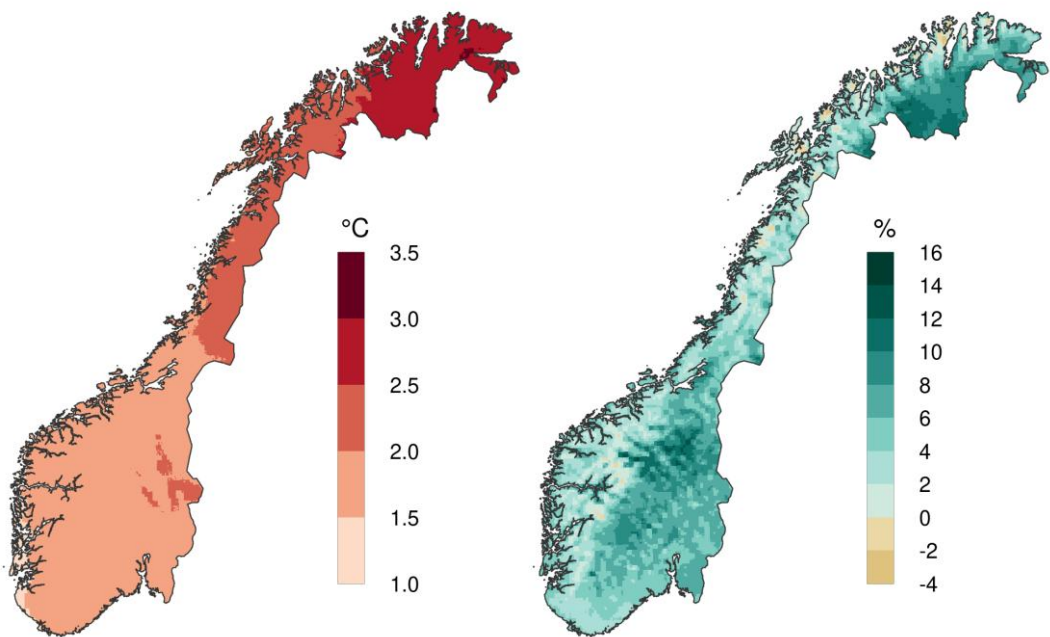
591

592

593

594

Looking at the spatial distribution of changes from the reference period 1991–2020 to the far future period 2071–2100 (Fig. 11), a generally larger increase in temperatures towards the North is apparent, with about one to two °C in the southern and two to three °C in the northern half of Norway. Precipitation is increasing as well with exceptions of some isolated areas along the coast and in the mountains. Generally, the precipitation increases are small and below +12%.



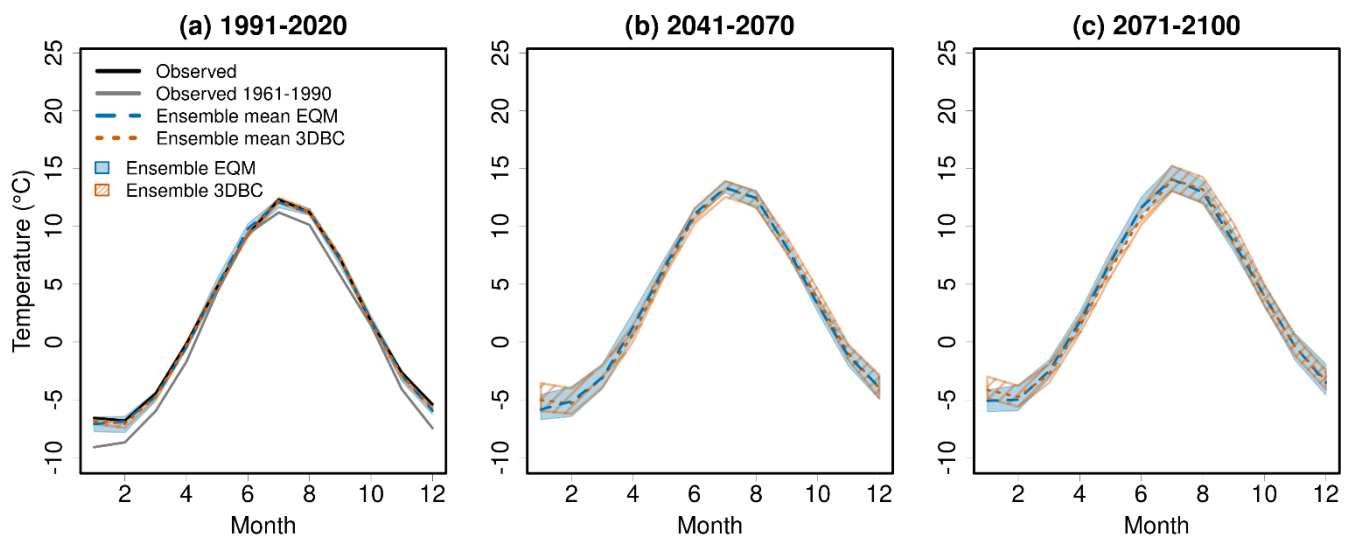
595

596

597

Figure 11: COR-BA-2025 ensemble mean changes in temperature (°C) (left) and relative changes in precipitation (%) (right) in the scenario period 2071–2100 relative to the reference period 1991–2020 under the RCP4.5 scenario for mainland Norway.

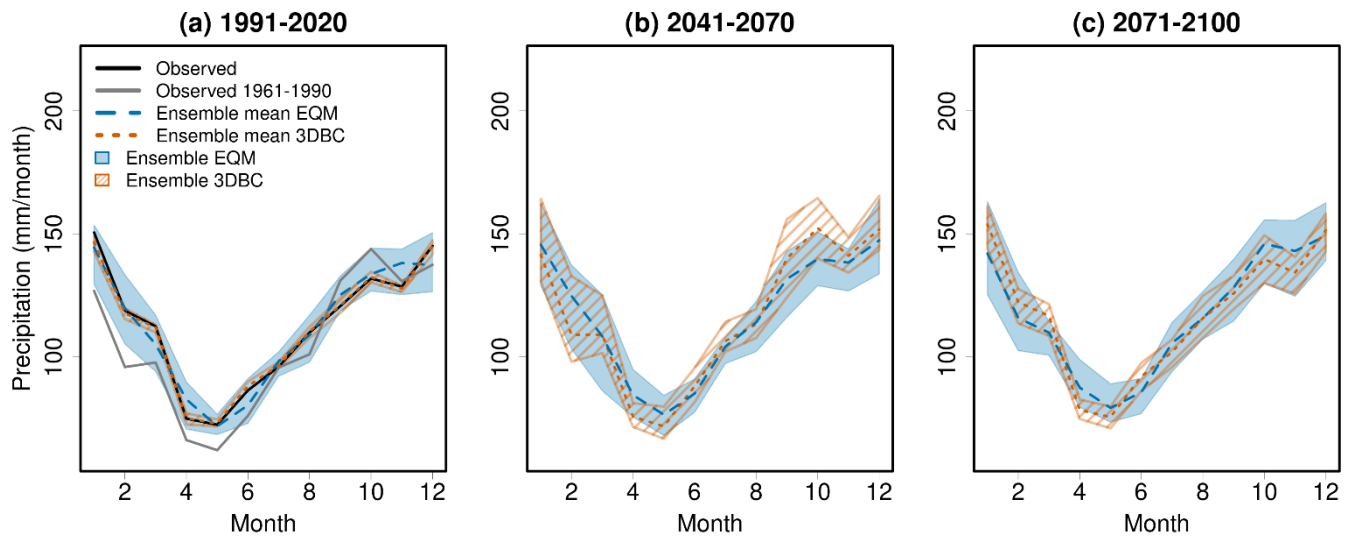
599 The effects of the two bias-adjustment methods on the preservation and altering of the seasonal climate change signals of the
 600 RCMs is shown in Fig. 6 and discussed in Section 5.3.2. Similarly, the two methods have different effects on the monthly
 601 climate change signal due to their design. While EQM is designed to preserve the monthly climate change signals, the 3DBC
 602 method is designed to provide spatial, temporal and inter-variable structures based on the reference data. However, as can be
 603 seen in Fig. 12 and 13, the shapes of the climatologies from EQM and 3DBC are similar and in agreement with the observed
 604 ones. As already seen for the seasonal changes (Fig. 6), precipitation and temperature changes in 3DBC are larger than in EQM
 605 in winter months (especially January and February) and smaller in spring and summer (April to June) for the far future period
 606 (2071–2100). For the near future (2041–2070), the difference in the changes from EQM and 3DBC are less systematic but
 607 3DBC shows a pronounced increase in autumn precipitation which is absent in EQM (Fig. 13). This shift in the 3DBC results
 608 can be traced back to its implementation: the rank structure from the reference years 1961-1990 are used for the 2041-2070
 609 period. Since the autumn precipitation in the period 1961-1990 has been large (Fig. 13a), this is imprinted on the mean annual
 610 cycle of the near future period. For the current climate (1991–2020), the 3DBC method results in climatologies that are similar
 611 for all models and thus a small ensemble-spread compared to the EQM data. This is especially true for precipitation (Fig. 13).



612

613 **Figure 12: 30-year mean monthly temperatures for Norway for different time periods using the EQM and 3DBC bias-adjusted**
 614 **climate projections under the RCP4.5 scenario. Black line: Observed temperature in 1991–2020. Grey line: Observed temperature**
 615 **in 1961-1990. Blue and orange lines: ensemble means of simulated temperature. Blue and orange striped areas: ensemble spread of**
 616 **10 projections.**

617



618
619 **Figure 13: The same as Fig. 12 but for precipitation.**

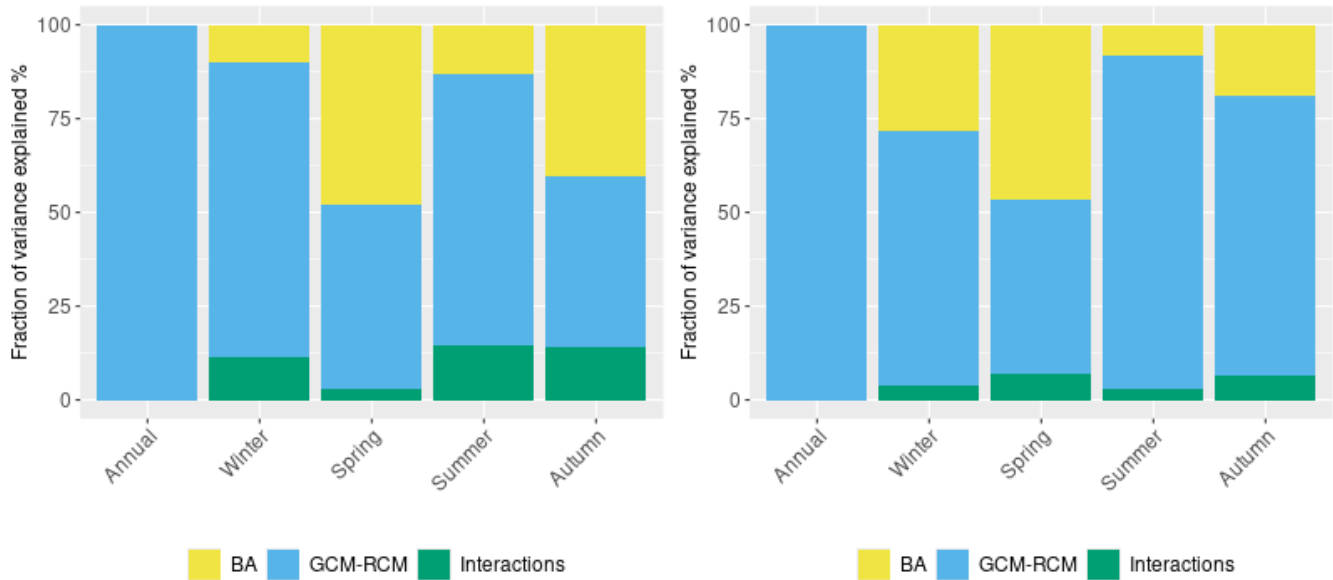
620 **7.3 Uncertainty analysis**

621 Besides the two different bias-adjustment methods, the various GCM-RCM combinations contribute to uncertainties in the
 622 climate projections. In this section, we analyse the contribution of these two uncertainty sources using the ANOVA method
 623 used by Vetter et al. (2017). Since each GCM is combined with different RCMs (see Section 4), we don't distinguish the
 624 GCMs and RCMs as different uncertainty sources here, but consider the GCM-RCM combinations as one uncertainty source.
 625 The two bias-adjustment methods are considered the second uncertainty source. The ANOVA method provides not only
 626 variations in the impact on temperature/precipitation from these two major sources, but also their interaction term. To avoid
 627 the bias caused by different sample sizes of the sources, the ANOVA was implemented for a number of subsamples, each of
 628 which includes two climate models and two bias correction methods, and then the obtained estimates of subsamples were
 629 averaged. For more explanation of the method and equations, please refer to Vetter et al. (2017).

630 Since our implementation of 3DBC conserves the annual changes from EQM, the annual fraction of variance from the ANOVA
 631 analysis (Fig. 14 and 15) is solely dependent on the GCM-RCM combination. On a seasonal scale, the largest contribution to
 632 temperature uncertainties still comes from the GCM-RCM combinations. However, for spring and autumn the bias-adjustment
 633 contribution can be of similar size, especially in the near future projections. Interactions between the two uncertainty sources
 634 are generally small.

635 For precipitation, the contribution to the overall uncertainty from the bias-adjustment methods is larger than the contribution
 636 from the climate models for spring and autumn in the near future. Also for the other two seasons, the different contributions
 637 are of similar size for the near future. Interestingly, for the far future, the contribution from the climate models is clearly larger

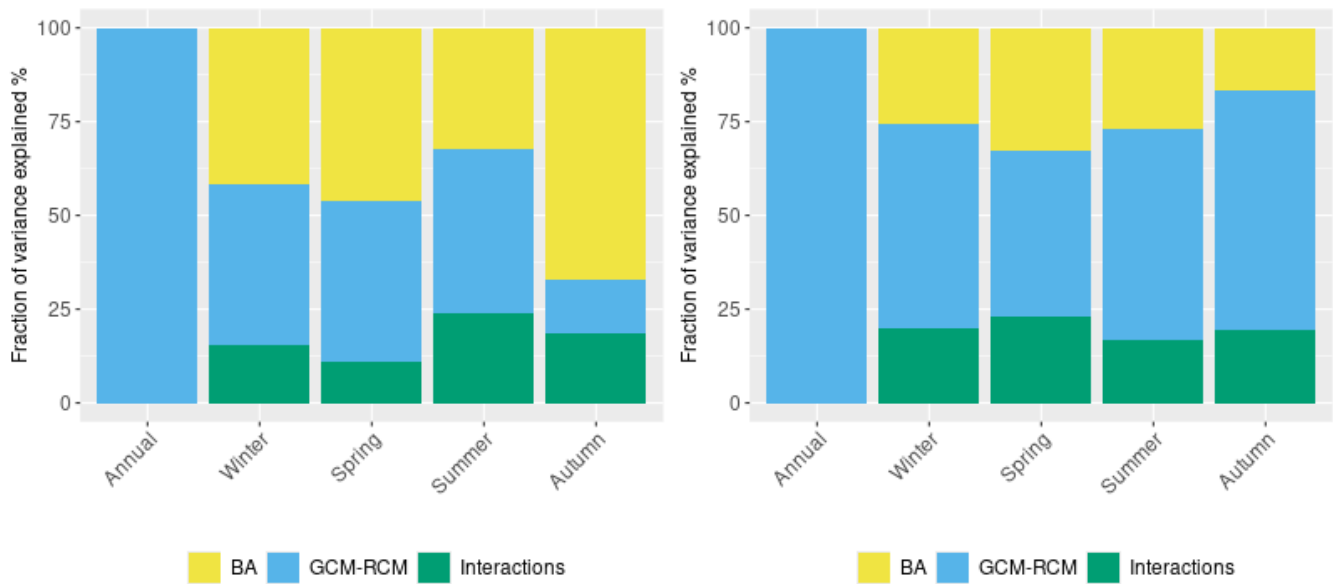
638 than the contribution from the bias-adjustment methods for all seasons. The interactions are larger than for temperature and
 639 can reach magnitudes similar to the single contributions. This is an effect of the two bias-adjustment methods resulting in
 640 seasonal change signals that differ more for precipitation than temperature, showing that results for temperature from a single
 641 bias-adjustment method are more robust than for precipitation. This is especially true for the near future.
 642



643

644 **Figure 14: the fraction of variance in projected temperature changes explained by bias-adjustment methods (BA), GCM-RCM**
 645 **combinations and their interactions for the near-future period (2041–2070, left) and far-future period (2071–2100, right).**

646



647

648

Figure 15: The same as Fig. 14 but for precipitation.

649

650

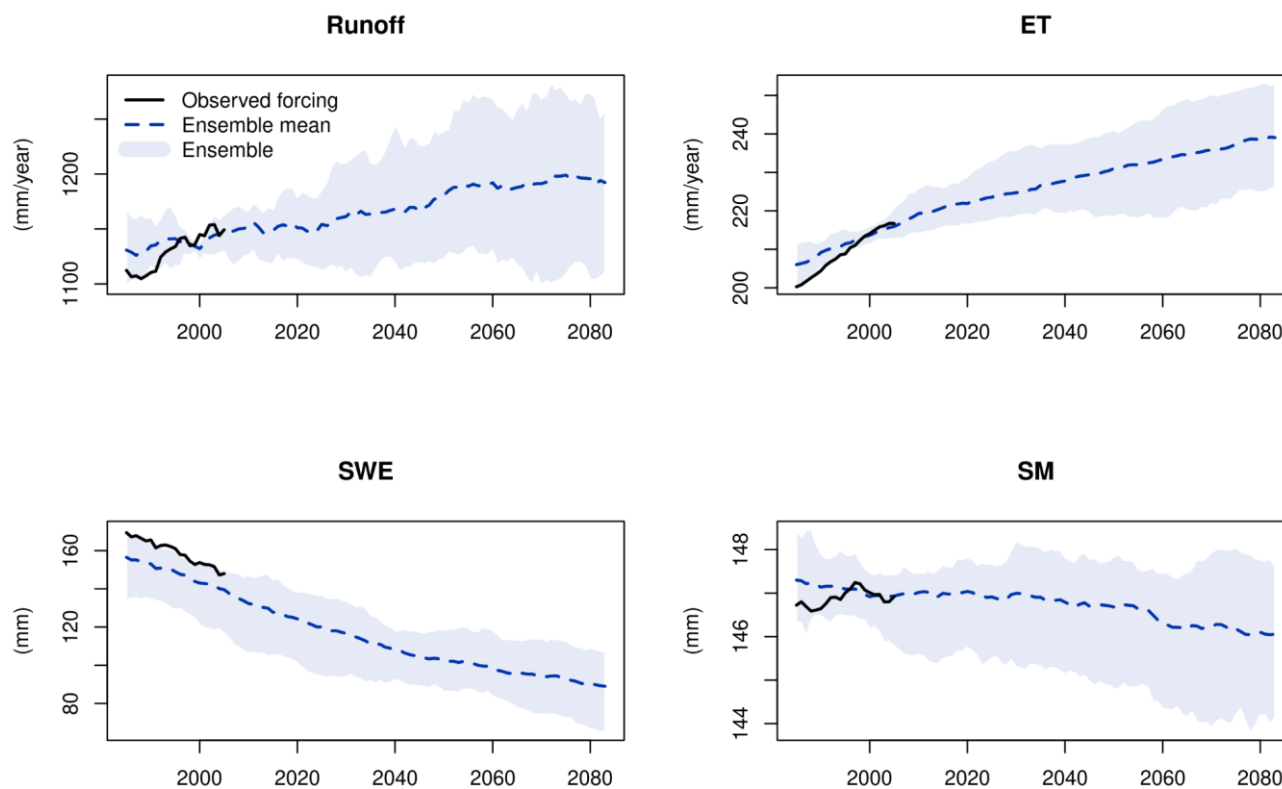
651

652

653

654

Our findings bring new insights into uncertainty attribution for seasonal projections, because most studies on uncertainty attribution are mainly targeted at annual values rather than seasonal ones, e.g. Paz and Willems (2022) and Lafferty and Sriver (2023). There are only a few uncertainty analyses for seasonal changes, but they did not find larger uncertainty associated with bias-adjustment methods than the variability within the model ensemble (Tong et al., 2021; Zhang et al., 2024). Our results highlight that bias-adjustment methods can be an important uncertainty source for seasonal projections and their seasonal effects should be considered in future studies.

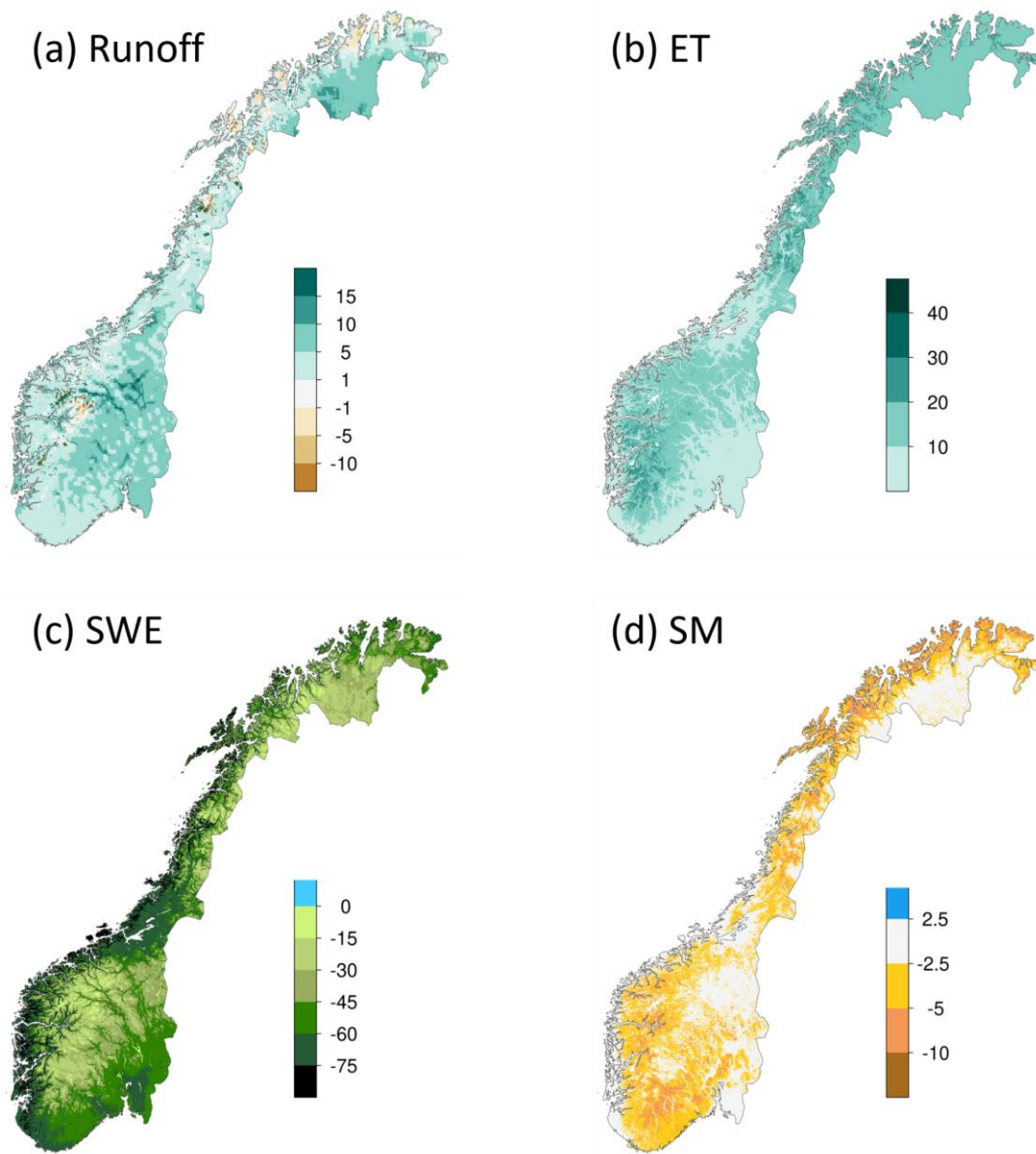


657
 658 **Figure 16: Simulated 30-year running means of annual runoff, evaporation (ET), mean snow water equivalent (SWE) and mean soil**
 659 **moisture (SM) driven by the ensemble of 20 climate projections (10 GCM-RCMs x 2 bias correction methods) under the RCP4.5**
 660 **scenario. The black line is the simulated water components driven by the observed forcing data.**

661 There are 20 hydrological projections for mainland Norway at 1km spatial resolution with daily time steps under the RCP4.5
 662 scenario from the distHBV-COR-BA-2025 dataset. Figure 16 shows the projected annual sum/mean of these variables from
 663 1971 to 2098 for mainland Norway. Both the ensemble means of runoff and evaporation have an increasing trend while the
 664 ensemble means of snow water equivalent and soil moisture tend to decrease towards the end of this century. The simulated
 665 runoff, evaporation, and soil moisture driven by the seNorge forcing data (black lines) are generally within the boundary of
 666 the 20 simulations in the historical period, and they have a good agreement with the ensemble mean around the year 2000. In
 667 addition, the spread of projections is reduced around the year 2000, as the bias-adjusted data matches the statistics of the
 668 observations better in the training period 1985-2014 than other periods. However, all snow water equivalent simulations are

669 generally underestimated compared with the simulated snow water equivalent driven by the seNorge data, indicating that snow
670 generation is not well reproduced. It is mainly due to inaccurate inter-variable, spatial and temporal dependence between the
671 bias-adjusted atmospheric variables when only the EQM method is used (see section 8.2).

672 Figure 17 shows the spatial distribution of the ensemble mean changes in the last scenario period (2071–2100) relative to the
673 reference period (1991–2020). In general, the increase in runoff is dominant in the whole country, except glacier retreat areas
674 around the glaciers and the coastal areas in the northern part of Norway. The increases are minor (<5%) or moderate (5–10%)
675 in most parts of the country and strong increase in runoff (> 10%) occurs mainly in the glacier areas, lakes and rivers as well
676 as some northernmost areas. Due to the warmer and wetter climate in the future, evaporation is projected to increase in the
677 whole country, especially in western and central Norway. In contrast, the annual mean snow water equivalent will decrease in
678 the whole country in the far future, with a strong decrease (<-75%) along the coast. Note that snow volumes along the coast
679 of Southern Norway are small in today's climate. The absolute decrease in annual mean snow water equivalent is not stronger
680 along the coast than mountainous areas. Soil moisture will decrease in most parts of the country due to the increase in
681 evaporation and earlier snow melt, and moderate to strong decreases (<-5%) are mainly found in some southern areas and the
682 coastal regions in the north.

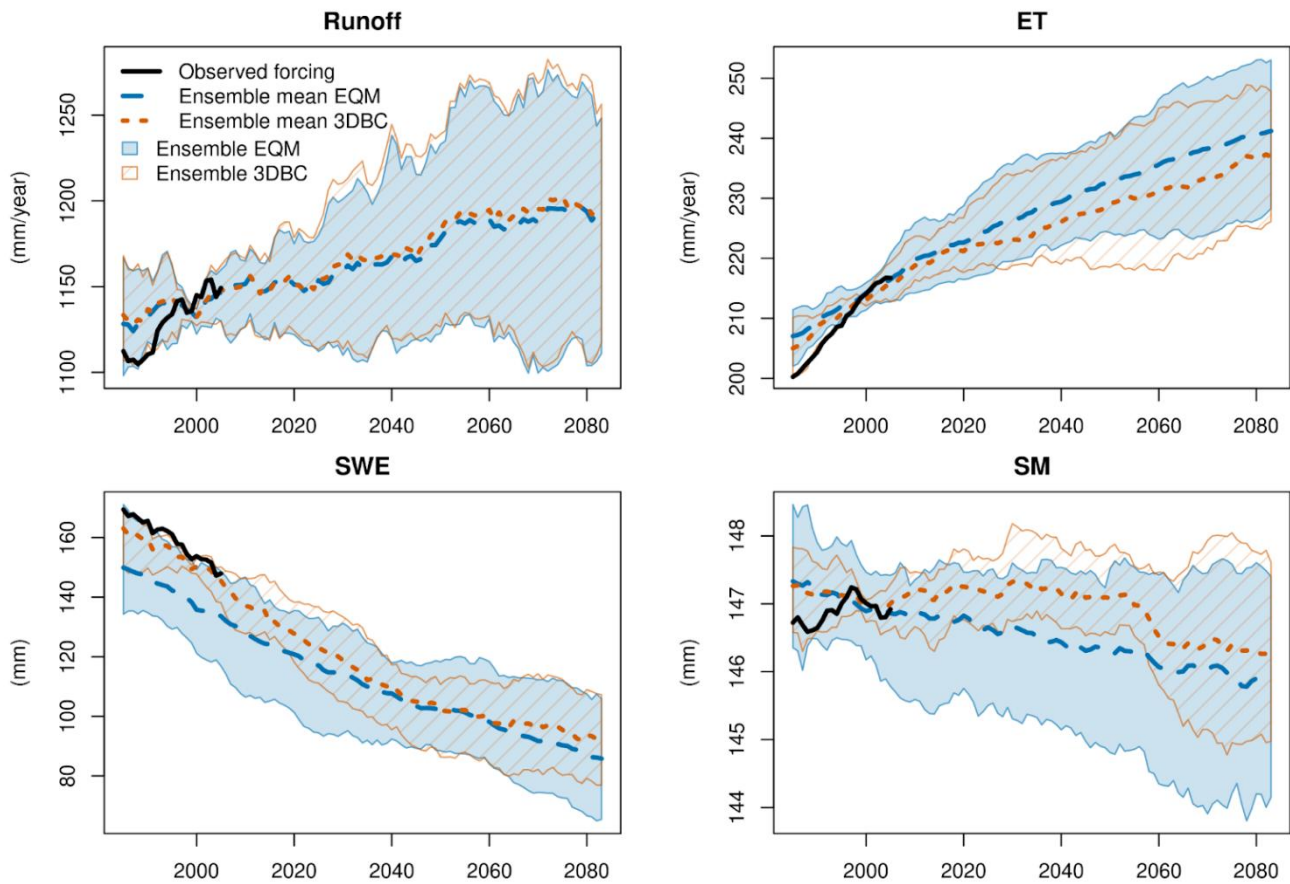


683
 684 **Figure 17: ensemble mean changes (%) in annual runoff (a), evaporation (ET) (b), snow water equivalent (SWE) (c) and soil moisture**
 685 **(SM) (d) in the scenario period 2071–2100 relative to the reference period 1991–2020 under the RCP4.5 scenario for mainland**
 686 **Norway.**

687 **8.2 Effects of the two bias-adjustment methods**

688 In this section, we provide a general overview of the effects of the bias-adjustment methods on hydrological projections. Figure
 689 18 shows again the projected annual sum/mean of hydrological variables from 1971 to 2098 for mainland Norway, but

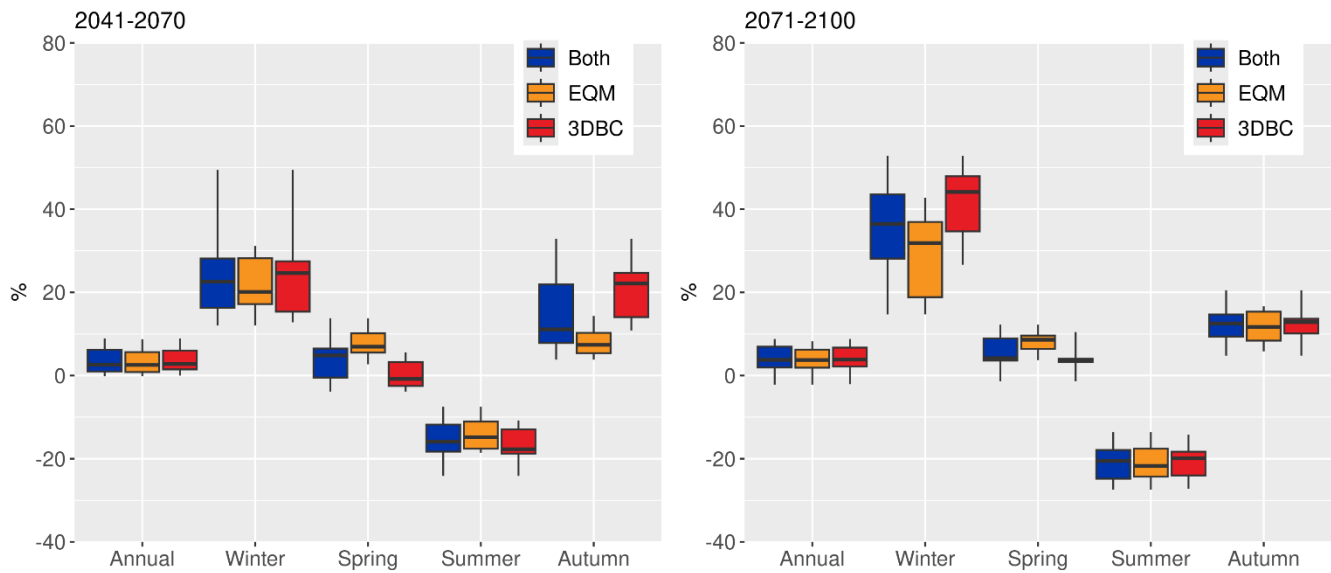
690 separating the projections between the two bias-adjustment methods. The results show that the two bias-adjustment methods
691 play a minor role on ensemble means as well as ensemble spread for runoff, evaporation and soil moisture, with the differences
692 between the bias-adjustment methods less than 10 mm/year for runoff and evaporation and less than 1 mm for soil moisture.
693 The ensemble mean of snow water equivalent using the 3DBC method has a better agreement with the results driven by
694 observed forcing data than the ensemble mean using the EQM method, which always leads to underestimation of snow water
695 equivalent in the historical period. In addition, the ensemble spread for snow water equivalent is narrower using 3DBC than
696 EQM, especially before 2040, indicating lower uncertainty of projections using 3DBC. However, it is interesting to see that
697 the snow water equivalent projections do not differ substantially after 2040 between the two bias-adjustment methods.
698 Although the correlation structures and temporal sequences in the 3DBC data for this period are still similar to the observed
699 ones in all models, different climate change signals in the RCMs lead to a larger overall spread in the driving variables,
700 particularly temperature (Fig. 10). Thus, the resulting snow water equivalent projections using the 3DBC data inherit the
701 general climate change signals and become similar to the EQM projections. The minor impact of bias-adjustment methods on
702 annual values also leads to similar spatial distributions of the changes in runoff, evaporation and soil moisture, but considerable
703 differences of changes in snow water equivalent are found along the coast and northmost Norway between the bias-adjustment
704 methods (Fig. S3 in Supplementary material).



705

706 **Figure 18: The same as Fig. 16 but the projections using different bias-adjustment methods are separated.**

707 Although the bias-adjustment methods affect the annual changes in runoff marginally, they lead to different seasonal runoff
 708 changes and their effects vary in scenario periods and seasons. Figure 19 shows the seasonal relative changes in runoff
 709 including all 20 projections, 10 projections using the EQM bias-adjustment method and 10 projections using the 3DBC method,
 710 respectively. In the near future, the largest difference in the ensemble median changes between the bias-adjustment methods
 711 is found in autumn (ca. 13%), followed by the difference in spring (ca. 8%), winter (ca. 5%) and summer (ca. 3%). The 3DBC
 712 method leads to higher runoff changes in winter and autumn, but lower runoff changes in spring and summer than the EQM
 713 method. As a result, the two methods lead to similar changes in annual changes. In the far future, the bias-adjustment methods
 714 mainly affect the runoff changes in winter and spring, resulting in a difference in median changes of 12% in winter and 5% in
 715 spring. There is almost no difference in median runoff changes between the methods in summer and autumn. These results
 716 indicate that the two bias-adjusted methods mainly affect the snow accumulation and melt processes, which occur in autumn,
 717 winter and spring in the near future and in winter and spring in the far future. In addition, 3DBC always leads to higher runoff
 718 in winter and lower runoff in spring than EQM in both scenario periods.



719

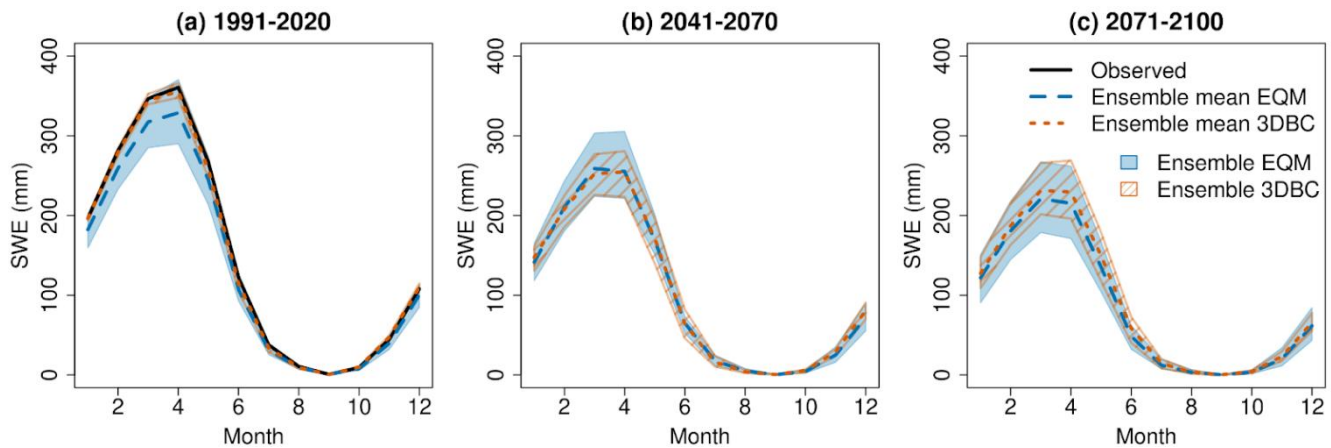
720

Figure 19: relative changes in runoff for different seasons in the scenario periods 2041–2070 (left) and 2071–2100 (right) relative to the reference period 1991–2020 under the RCP4.5 scenario for mainland Norway.

721

722

723



724

725

Figure 20: Simulated monthly snow water equivalent (SWE) for mainland Norway using the EQM and 3DBC bias-adjusted climate projections.

726

727

728

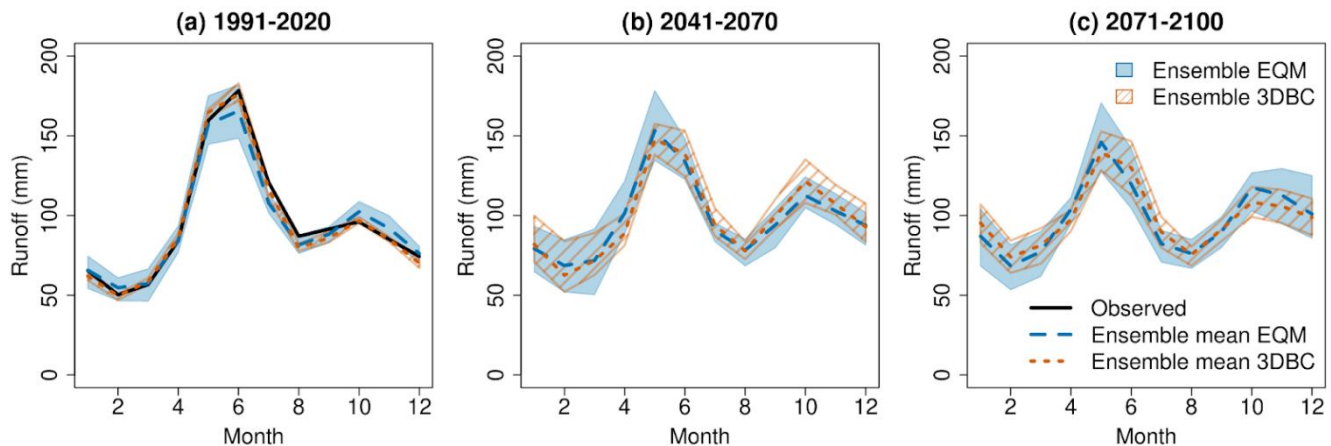
In order to illustrate the effects of the two bias-adjustment methods on snow processes, we compared the monthly snow water equivalent in the historical and scenario periods driven by different bias-adjusted projections as well as the ones driven by the observed forcing data (Fig. 20). In the historical period, the ensemble mean of monthly snow water equivalent driven by the 3DBC bias-adjusted projections agrees well with the simulated one driven by the observed forcing data. The EQM bias-

730

731 adjusted simulations generally lead to underestimation of monthly snow water equivalent, especially in March and April,
732 similar to the findings by Meyer et al. (2019). In addition, the historical snow simulations using the EQM method vary
733 substantially between climate models, while all bias-adjusted climate projections using the 3DBC method lead to similar
734 monthly SWE, indicating more robust snow projections in the historical period using the 3DBC method than the EQM method.

735 The two bias-adjusted methods also affect the projected changes in snow water equivalent in the scenario periods, especially
736 in the near future. The ensemble mean of monthly snow projections using the 3DBC methods show average decreases of about
737 44 and 55 mm/month in the near and far future periods relative to the reference period respectively, while the ensemble mean
738 using the EQM method decreases by 33 and 50 mm/month on average in the near and far future periods, respectively. It is due
739 to higher snow water equivalent in the historical period and lower snow water equivalent in the near future using the 3DBC
740 bias-adjusted projections than those using the EQM projections. However, the differences in snow water equivalent between
741 the near and far-future periods are smaller using the 3DBC than the EQM method, leading to closer agreement on snow water
742 equivalent changes in the far future between the two methods. The uncertainty bounds of snow projections using the 3DBC
743 method are still smaller than the uncertainty bounds using the EQM method in both future periods, but the differences in
744 uncertainty bounds between the two methods is less substantial than the ones in the historical period.

745



746

747 **Figure 21: The same as Fig. 20 but for runoff.**

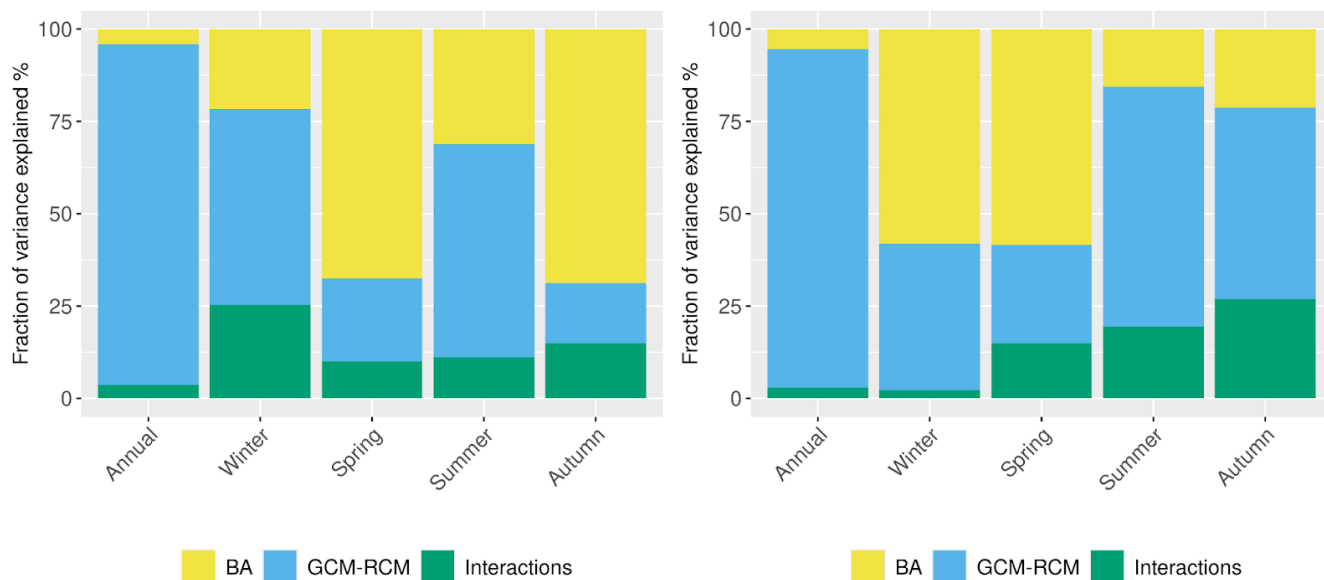
748 Partly due to different snow simulations, the monthly runoff projections also differ between the two bias-adjustment methods
749 (Fig. 21). In the historical period, the simulated runoff using the 3DBC bias-adjusted climate simulations also agrees well with
750 the simulated runoff using observed forcing data, while the simulations using the EQM bias-adjusted climate simulations
751 underestimate runoff from June to July that is generated by snow melt, mainly due to less snow storage in winter and spring
752 (Fig. 20). There is also an overestimate of runoff from October to November using the EQM bias-adjusted climate simulations,

753 indicating that other hydrological processes besides snow are also affected by the inaccurate spatial and temporal correlations
 754 of climate variables. Similarly, the runoff simulations using the EQM bias-adjusted climate projections have larger uncertainty
 755 bounds than the ones using the 3DBC projections.

756 In the future periods, the runoff projections using the 3DBC method show larger increase and decrease in monthly changes
 757 relative to the historical period than using the EQM ones. In addition, the 3DBC bias-adjusted climate projections lead to
 758 higher runoff in autumn in the near-future than in the far-future while the EQM projections show contradicting changes.
 759 Different from the snow projection uncertainty, the runoff uncertainty using the 3DBC method is not always smaller than the
 760 one using the EQM method in all months. In addition, the large runoff uncertainty in the historical and future periods does not
 761 lead to large uncertainty of runoff changes. As shown in Fig. 19, the uncertainty bounds of runoff changes using the 3DBC
 762 method is not substantially larger than the uncertainty of changes using the EQM method.

763 8.3 Uncertainty analysis

764



765

766 **Figure 22: the fraction of variance in runoff change projections explained by bias-adjustment methods (BA), GCM-RCM**
 767 **combinations and their interactions for the near-future period (2041-2070) (left) and far-future period (2071-2100).**

768 Similar to temperature and precipitation, we assessed the contribution of the two bias-adjustment methods and GCM-RCM
 769 combinations to the uncertainty in the runoff projections. Figure 22 shows the fraction of variance from the ANOVA analysis
 770 for the GCM-RCM combinations, bias-adjustment methods and their interactions for the two future periods. For both periods,

771 it is obvious that the climate model combinations contribute to the majority of the annual runoff change variance (> 90%).
772 However, the bias-adjustment methods play important roles in the seasonal runoff changes, especially in spring and autumn in
773 the near future and in the winter and spring in the far future, explaining more than 50% of the runoff change variance. For
774 summer, the climate model combinations are always the major uncertainty source, explaining more than 50% of the total runoff
775 change variance. These results highlight the effects of bias-adjustment methods on seasonal runoff change projections.

776 **9 Discussion**

777 **9.1 Limitations of the methodology**

778 In this study, we present the whole modelling chain that produces the updated national ensembles of climate and hydrological
779 projections for the new Climate in Norway report CiN-2025 (Dyrddal et al., 2025). This modelling chain includes selection of
780 emission scenarios and climate models, downscaling and bias-adjustment methods and hydrological models. Although we
781 have made a number of substantial improvements in each component of the modelling chain, there are still limitations and
782 weaknesses in the methodology, which require further development for future climate impact assessments.

783 The first component in the modelling chain is to select appropriate emission scenarios and climate projections from a large
784 ensemble of GCM and RCM outputs manageable throughout the complete chain. As a national climate assessment report
785 following the sixth IPCC report, it would have been ideal to apply the most updated emission scenarios (i.e., the SSPs) and the
786 corresponding climate projections. However, due to the long time needed to make the newest RCM results available within
787 the CORDEX framework and the time limit of the national report, we had to apply the climate projections corresponding to
788 the fifth IPCC report for the low- and median emission scenarios (RCP scenarios). Complements of the national climate
789 projections for SSP emission scenarios are expected in the future to provide up-to-date knowledge on climate change impacts.

790 Since the EURO-CORDEX ensemble for the RCP scenarios is now much larger than for CiN-2015, the climate projections
791 for CiN-2025 are more representative of the full range of climate changes ensembles. However, the restriction to ten models
792 per scenario stemming from the complete modelling chain still partly limits the representativeness of the full possible outcome
793 and model variability. In CiN-2025, this limitation is taken into account for temperature and precipitation using results from
794 empirical-statistical downscaling (ESD) of the complete set of available GCMs. The ESD results are shown in the CiN-2025
795 report but not in this study as our focus is on the complete modelling chain. A detailed description of the ESD method used in
796 CiN-2025 is given in Benestad et al. (2025).

797 RCMs are still subject to general limitations of model simplifications, such as internal parameterizations and spatial resolution.
798 Further, some technical limitations remain in the RCM outputs, for example, some models provide outputs for 360 days per
799 year, no leap year days or start in 1970 and end in 2098. This brings challenges for impact models and requires pre-processing

800 before bias-adjustment. In addition, the historical period simulated by the RCMs does not cover the current standard normal
801 period (1991–2020). This is a drawback since it is easier for the general public to compare the climate change signals with
802 respect to the climate normal than other non-standard periods (e.g., 1976–2005). Although the use of the first few years from
803 the scenario projections as reference period is not optimal, and the choice of the reference period can lead to different climate
804 changes signals (Liersch et al., 2020), the use of the most recent standard normal period improves the public acceptance and
805 understandability substantially, which is most important for the target users of a national report such as CiN-2025.

806 As the second component of the modelling chain, downscaling and bias-adjustment methods allow presenting projected climate
807 and hydrological changes at a spatial resolution of 1x1 km for the complex topography of Norway. Providing such high
808 resolution data needs high computational costs and makes it challenging to test and apply a large number of bias-adjustment
809 methods. Hence, we only selected EQM as the bias-adjustment method as it is robust for different climatological regimes and
810 well established. The 3DBC method is further applied on the EQM bias-adjusted variables to improve the inter-variable, spatial
811 and temporal dependencies. This multivariate bias-adjustment method indeed improves the hydrological projections,
812 especially for snow simulations, and reduces the uncertainty range, especially in the reference period. However, the 3DBC
813 method (Section 5.3) leads to different climate change signals compared to the original RCM signals on sub-annual scales
814 because it imposes temporal dependency structures on the future projections similar to the ones from the reference datasets.
815 This may be considered a weakness of the approach and more evaluation and development of multivariate bias-adjustment
816 methods are required to further improve the existing methods. As discussed in François et al. (2020), the choice of method
817 may differ from case to case, depending on which statistical properties from the RCMs need to be preserved or corrected.
818 Based on our findings, users of the bias-adjusted data may select the appropriate dataset depending on their needs, or simply
819 consider the two methods being equal, resulting in a broader ensemble.

820 In this study, RCM outputs have firstly been interpolated to the resolution of the observations (1 km) using the nearest-
821 neighbour method and then bias-adjusted on that resolution. However, users should not overinterpret projected changes which
822 are finer than the native RCM resolution (~12.5 km) as the resolving power of the RCM sets the natural lower limit on which
823 local-scale physical processes can be considered. Maraun (2013) has shown that the quantile mapping method cannot resolve
824 this scale mismatch. This effect might be less important for temperature than precipitation as temperature usually has a much
825 higher spatial coherence while precipitation is more subjected to small-scale variability. Although generally both the EQM
826 and the 3DBC methods in our setup do not bring in climate change signals below the RCM resolution, some artifacts might be
827 introduced which do not represent true local, small-scale climate changes.

828 Regarding hydrological models, both the potential evaporation module and glacier modelling have been improved compared
829 to the model used in CiN-2015. The Penman-Monteith method improves evaporation estimates under climate scenarios by
830 considering more climate variables and representing different land cover types (Huang et al., 2026), while the dynamic glacier
831 modelling by DEW successfully avoids unrealistically high runoff from the glacier retreat areas under a warming climate.

832 However, the simulations of distHBV may still suffer equifinality problems due to a large number of calibration parameters,
833 which do not represent the physical characteristics of specific land use and soil types. In addition, we reclassify the soil types
834 into five major groups in order to reduce the number of calibration parameters related to soil processes. This may lead to
835 unreliable simulations for the areas where the soil condition is largely different from the major soil types. Therefore, both the
836 calibration procedure and the spatial representation of soil physical characteristics are expected to improve in the future
837 national applications.

838 Last but not least, vegetation types and characteristics are static in our hydrological modelling under climate change scenarios,
839 but the changes in vegetation characteristics are expected under a warming climate. Huang et al. (2025a) assessed the effects
840 of forest growth and forest management on water resources in six Norwegian catchments under the RCP2.6 and RCP4.5
841 emission scenarios. They found that forest growth would offset the increase in runoff in the catchments, where the deciduous
842 forest is dominant. It implies that the runoff in the deciduous forest areas, especially in North Norway, may be overestimated
843 in our present runoff projections. For the next generation CiN report, the land use and vegetation change scenarios should be
844 included in the hydrological modelling if such scenarios are available.

845 **9.2 Comparison of results between the old and new national reports**

846 The improved modelling chain generated updated climate and hydrological projections for Norway, which resulted in slightly
847 different climate change signals and climate impacts compared to the analysis in the old national report. Under the RCP4.5
848 scenario, the projections for the old and new national reports agree on the direction of change, but CiN-2025 projections display
849 a smaller increase in annual temperature (ensemble mean of 2.0 °C) and precipitation (ensemble mean of 6%) than the
850 ensemble means in CiN-2015 (2.7 °C and 8% increase in temperature and precipitation respectively) at the end of the century.
851 In addition, the ensemble spread in CiN-2025 is narrower than in CiN-2015, indicating more robust climate change signals.
852 However, these differences are caused not only by the new selection of climate models, but also by the selection of the reference
853 period. In CiN-2015, 1971–2000 was used as the reference period while in CiN-2025, it is 1991–2020. As temperature has
854 already risen considerably in recent decades in Norway, annual mean temperature is higher in 1991–2020 than in 1971–2000,
855 and the differences in temperature between the periods 2071–2100 and 1991–2020 are consequently more moderate than those
856 between 2071–2100 and 1971–2000. In contrast, a larger increase in runoff is seen in CiN-2025 projections than in the previous
857 one, mainly due to the improved evapotranspiration routine in the hydrological model (Huang et al., 2026).

858 Another major difference between the old and new national report is that CiN-2025 selected SSP3-7.0 as the high-emission
859 scenario, which assumes lower emission than RCP8.5 used in CiN-2015. Under SSP3-7.0, the ensemble mean increases in
860 annual mean temperature, precipitation and runoff are 3.4 °C, 11% and 10% in 2071-2100 relative to 1991-2020, respectively
861 (Fig. S4, S5 and S16 in Supplementary materials). These increases are also smaller than the ones in 2071-2100 relative to

1971-2000 under the RCP8.5 scenario, shown in the old national report. Hence, users who have made computations based on the CiN-2015 projections, should notice these differences and justify whether their computations should be updated or not.

9.3 The effects of bias-adjustment methods under the high-emission scenario SSP3-7.0

This paper comprehensively compared the two bias-adjustment methods applied to EURO-CORDEX RCP4.5 simulations and found that the two methods can lead to considerable differences in seasonal changes and snow simulations under the moderate-emission scenario. However, the impact of the bias-adjustment methods may not only vary between climate models and future periods but also between emission scenarios. Thus, results for the same comparison between the two bias-adjustment methods under SSP3-7.0 are included in the Supplementary material (Figures S6-S19). Although the magnitudes of the projected changes between SSP3-7.0 and RCP4.5 differ, the general effects and differences between the two bias-adjustment methods are similar. One interesting aspect is a generally better agreement of the SSP3-7.0 ensemble mean temperature and precipitation with the observed values than in the RCP4.5 simulations during the reference period (Fig. S4).

For hydrological projections, 3DBC still provides better historical simulations than EQM under the SSP3-7.0 scenario, but the difference in future projections varies between the bias-adjustment methods and seasons. Considerable differences of ensemble mean changes in runoff are found in all seasons in the near future and in winter in the far future. The ensemble spreads of monthly projections for snow water equivalent and runoff are similar between 3DBC and EQM for almost all months, indicating that 3DBC does not help to reduce the projection uncertainty substantially under extremely warm conditions.

9.4 Application

Despite the limitations mentioned above, the COR-BA-2025 and distHBV-COR-BA-2025 datasets generated by the presented modelling chain provide the most updated, comprehensive and detailed hydrometeorological projections for mainland Norway. These national projections serve as the scientific basis for research on climate change impacts in Norway. The gridded hydrometeorological projections from CiN-2015 have already been used to derive new indices for specific application, e.g. snow-dependent tourism (Kuya et al., 2024; Mayer et al., 2023), reindeer husbandry (Hanssen-Bauer et al., 2022), frost decay exposure on building projects (Gaarder et al., 2024) and road maintenance (Nilsen et al., 2021). In addition to impact modellers, who represent an advanced user group, NCCS aims at providing tailored information for practical climate adaptation. Products derived from the national projections have also been widely used in local planning, mainly because government guidelines (Norwegian Government, 2024) required municipalities to take climate change into account in planning. Climate factsheets (Hisdal et al., 2021) provided the most relevant information to guide the climate adaptation work, and were pointed out as a core reference in government guidelines. See Nilsen et al. (2022) for an overview of the steps from climate model output to actionable climate information.

891 Besides the possibility to update existing applications that used the gridded dataset from CiN-2015, the new COR-BA-2025
892 and distHBV-COR-BA-2025 datasets provide additional variables, such as wind speed, pressure, evaporation, radiation and
893 relative humidity, each bias-adjusted both with EQM and 3DBC. This improves the utility of the dataset for e.g., ecological
894 modelling (see Pirk et al., 2023 for an example). It is expected that the new dataset will facilitate use in an even wider range
895 of applications in the coming years, for climate change impacts on e.g., glaciers, drought, landslides and water availability.
896 Further work will involve user groups such as municipal planners to co-create climate services based on the
897 hydrometeorological projections presented.

898 In principle, we suggest using the full ensemble projections with both bias-adjustment methods to account for the uncertainty
899 of the whole modelling chain. But in practice, users may want to select a subset of climate models and one bias-adjustment
900 method to reduce the computational cost of further applications. As the users may be only interested in parts of Norway and
901 the performance of climate models and bias-adjustment methods vary in space and time, we are not able to give a
902 straightforward suggestion on the subset of climate models and bias-adjustment methods based on the national analysis.
903 However, the methodology as well as the analysis in this paper provides examples of selecting models and bias-adjustment
904 methods. In order to select a subset of climate models, the users can analyze the climate signals for their study area and periods
905 as in Fig. 3 and then select the models based on the study purpose, e.g., studies aiming to assess the driest and warmest climate
906 conditions or the wettest and coldest conditions in the near or far future. Based on the selected models, the users can further
907 assess the seasonal trends for their study area and periods using both EQM and 3DBC projections as in Fig. 6. If the trends are
908 comparable between the two bias-adjustment methods, the 3DBC adjusted projections can be preferred, especially when the
909 study is focused on seasonal changes and snow processes. Otherwise, we strongly recommend to use the projections adjusted
910 by EQM and 3DBC to account for the uncertainty of bias-adjustment methods.

911 Finally, we should note that the gridded datasets distHBV-COR-BA-2025 are not designed to use for flood indices, or climate
912 change allowances for floods because distHBV was calibrated against many catchments simultaneously. Instead, the outputs
913 from specific flood models should be used (Lawrence, 2020; Carr et al., 2023). The flood models include two lumped
914 hydrological models and were calibrated against observed discharges for each catchment separately. Hence, the flood models
915 produce more reliable estimates of high (and low) flow for specific catchments.

916 **10 Conclusions**

917 In this study, we present the whole modelling chain behind the production of updated national ensembles of climate and
918 hydrological projections for the official “Climate in Norway” assessment report. We also provide insight into the
919 hydrometeorological projections, which we termed COR-BA-2025 (standing for CORDEX-Bias Adjusted, updated in 2025)
920 for climate projections and distHBV-COR-BA-2025 for hydrological projections, and analyse their uncertainties. The

921 modelling chain (Fig. 2) includes the selection of GCM-RCM combinations for Norway from a large ensemble of EURO-
922 CORDEX simulations, the application of two bias-adjustment methods and distributed hydrological modelling including a
923 physically-based potential evaporation approach and a dynamic glacier model. Compared to the previous national assessment
924 report, the new climate projections are considered more representative for Norway due to a larger ensemble of EURO-
925 CORDEX simulations taken into account and a systematic analysis of the projections.

926 A multivariate bias-adjustment method has been applied for the first time over the whole of Norway for the complete
927 atmospheric dataset consisting of nine variables. This new method leads to more consistent data in space, time and between
928 variables, and to more robust hydrological simulations than the univariate empirical quantile mapping method (especially for
929 snow and in the reference period), but it does not preserve climate change signals on a sub-annual scale. However, the
930 uncertainty ranges of runoff change projections are not significantly different between the two bias-adjustment methods,
931 especially at the annual scale. An uncertainty analysis shows that the climate projections are the major source of uncertainty
932 for annual runoff change, while the selection of the bias-adjustment method plays an important role on seasonal changes.

933 Despite the advancement in the presented methodologies and modelling chain, there is still room for further improvement in
934 future climate impact assessment studies. Currently we foresee that additional emission scenarios and GCM-RCM
935 combinations from the EURO-CORDEX initiative will be evaluated and the bias-adjustment methods will be further developed
936 to overcome the current limitations. In addition, the calibration procedure and the calibration parameters in the hydrological
937 modelling will be further improved using advanced machine learning techniques. If possible, the land use and vegetation
938 changes scenarios should also be considered in hydrological modelling.

939 The methodological description provided here serves as core knowledge for any further application of the gridded products,
940 which are expected to be used in a wide range of climate impact assessments and development of climate adaptation strategies
941 in Norway. We have thrived to meet the FAIR principles (Wilkinson et al., 2016) for data management. Thus, the complete
942 COR-BA-2025 and distHBV-COR-BA-2025 datasets (Wong et al. 2025) are findable and accessible through the Arctic Data
943 Centre (adc.met.no) at <https://doi.org/10.21343/0k90-6w67>. The data is stored in NetCDF format following the attribute
944 convention for data discovery (ACDD version 1-3, https://wiki.esipfed.org/Attribute_Convention_for_Data_Discovery_1-3)
945 and the climate and forecast metadata conventions (CF version 1.10, Eaton et al., 2022). The code and data are reusable, being
946 open source with non-restrictive licenses.

947 **Code availability**

948 The code of distHBV is available at <https://doi.org/10.5281/zenodo.17531118> (Beldring, 2025a)

949 The code of DEW is available at <https://doi.org/10.5281/zenodo.17530242>, (Beldring, 2025b)

950 The R source code of the 3DBC implementation used in this work is available at <https://doi.org/10.5281/zenodo.15260334>
951 (Dobler, 2025).

952 EQM implementation used the functions *fitQmapQUANT* and *doQmapQUANT* from R package *qmap* which is available at
953 <https://doi.org/10.32614/CRAN.package.qmap> (Gudmundsson, 2025).

954 **Data availability**

955 The **COR-BA-2025** and **distHBV-COR-BA-2025** bias-adjusted daily high-resolution climate and hydrological projections
956 for Norway are freely available at the Arctic Data Centre (adc.met.no) under <https://doi.org/10.21343/0k90-6w67> (Wong et
957 al., 2025).

958 The reference datasets used in the modelling chain are available at <https://doi.org/10.21343/gbq0-4t97> (Huang et al., 2025b).

959 **Author contribution**

960 SM, SLS, TL, WKW and AD performed the analysis of climate model selections and collected the RCM data. WKW and AD
961 designed the bias-adjustment experiments and methods and carried them out. IH modified the model code distHBV and IH
962 and SH performed the simulations. SB and KM developed the model code DEW, designed the experiments of DEW and GR
963 performed the simulations. SH prepared the manuscript with contributions from all co-authors. AVD, HOH, IBN and SJB
964 coordinated the whole project.

965 **Competing interests**

966 The authors declare that they have no conflict of interest.

967 **Acknowledgement**

968 We acknowledge the World Climate Research Programme, the CORDEX Science Advisory Team (SAT) - coordinating body
969 of CORDEX, and the Working Group on Coupled Modelling (WGCM) - responsible panel for CMIP5 and CMIP6. We thank
970 the CORDEX climate modeling groups (listed in Table 1 and S1) for producing and making available their model output,
971 CMIP5 and CMIP6 for providing the driving data, the Earth System Grid Federation (ESGF) for providing access, and the
972 multiple funding agencies who support CORDEX, CMIP and ESGF.

973 **Financial support**

974 This article was funded by the Norwegian Centre for Climate Services, and thus supported by the Norwegian Environment
975 Agency and the Ministry of Climate and Environment in addition to in-kind contributions from the Norwegian Water
976 Resources and Energy Directorate, NORCE and the Norwegian Meteorological Institute.

977 **References**

978 Ahlstrøm, A., Bjørkelo, K., and Frydenlund, J.: AR5 klassifikasjonssystem - klassifikasjon av arealressurser, Skog og
979 landskap, rapport nr. 6/2014, 38 pp. <http://hdl.handle.net/11250/2440173>, 2014.

980 Alifu, H., Hirabayashi, Y., Imada, Y., and Shiogama, H.: Enhancement of river flooding due to global warming, *Sci Rep*, 12,
981 20687, <https://doi.org/10.1038/s41598-022-25182-6>, 2022.

982 Andreassen, L. M., Huss, M., Melvold, K., Elvehøy, H. og Winsvold, S. H.: Ice thickness measurements and volume
983 estimates for glaciers in Norway. *Journal of Glaciology*, 61(228), 763-775. <https://doi.org/10.3189/2015JG14J161>, 2015.

984 Astagneau, P. C., Wood, R. R., Vrac, M., Kotlarski, S., Vaittinada Ayar, P., François, B., and Brunner, M. I.: Impact of bias
985 adjustment strategy on ensemble projections of hydrological extremes. *Hydrol. Earth Syst. Sci.*, 29, 5695–5718,
986 <https://doi.org/10.5194/hess-29-5695-2025>, 2025.

987 Beck, H. E., Zimmermann, N. E., McVicar, T. R., Vergopolan, N., Berg, A., and Wood, E. F.: Present and future Köppen-
988 Geiger climate classification maps at 1-km resolution, *Sci Data*, 5, 180214, <https://doi.org/10.1038/sdata.2018.214>, 2018.

989 Beldring, S.: Distributed element water balance model system. *Norwegian Water Resources and Energy Directorate, Report*
990 *no. 4/2008*, 40 pp. https://publikasjoner.nve.no/report/2008/report2008_04.pdf
991 https://github.com/DistributedElementWaterModel/Version_3.03, 2008.

992 Beldring, S.: nve-sbe/DistributedHbv: v_1 (v_1), Zenodo, <https://doi.org/10.5281/zenodo.17531118>, 2025a.

993 Beldring, S.: DistributedElementWaterModel/Version_3.03: v_1 (v_1), Zenodo, <https://doi.org/10.5281/zenodo.17530242>,
994 2025b.

995 Beldring, S., Engeland, K., Roald, L. A., Sælthun, N. R., and Voksø, A.: Estimation of parameters in a distributed precipitation-
996 runoff model for Norway, *Hydrology and Earth System Sciences*, 7, 304–316, <https://doi.org/10.5194/hess-7-304-2003>, 2003.

997 Benestad, R. E., Parding, K. M., and Dobler, A.: Downscaling the probability of heavy rainfall over the Nordic countries,
998 *Hydrol. Earth Syst. Sci.*, 29, 45–65, <https://doi.org/10.5194/hess-29-45-2025>, 2025.

999 Bremnes, J. B.: Probabilistic wind power forecasts using local quantile regression, *Wind Energy*, 7, 47–54,
1000 <https://doi.org/10.1002/we.107>, 2004.

1001 Bright, R. M., Eisner, S., Lund, M. T., Majasalmi, T., Myhre, G., and Astrup, R.: Inferring Surface Albedo Prediction Error
1002 Linked to Forest Structure at High Latitudes, *Journal of Geophysical Research: Atmospheres*, 123, 4910–4925,
1003 <https://doi.org/10.1029/2018JD028293>, 2018.

1004 Bürger, G., Sobie, S. R., Cannon, A. J., Werner, A. T., and Murdock, T. Q.: Downscaling Extremes: An Intercomparison of
1005 Multiple Methods for Future Climate, *Journal of Climate*, 26, 3429–3449, <https://doi.org/10.1175/JCLI-D-12-00249.1>, 2013.

1006 Carr, S., Lawrence, D., Skaugen, T., and Wong, W. K.: Projected future changes in peak flows and implications for climate
1007 change allowances, NVE report nr. 26/2023, The Norwegian Water Resources and Energy Directorate, Oslo, Norway,
1008 https://publikasjoner.nve.no/rapport/2023/rapport2023_26.pdf, 2023.

1009 Cannon, A.J., Sobie, S.R. and Murdock, T.Q.: Bias Correction of GCM Precipitation by Quantile Mapping: How Well Do
1010 Methods Preserve Changes in Quantiles and Extremes? *Journal of Climate*, 28, 6938-6959, [https://doi.org/10.1175/JCLI-D-](https://doi.org/10.1175/JCLI-D-14-00754.1)
1011 [14-00754.1](https://doi.org/10.1175/JCLI-D-14-00754.1), 2015.

1012 CH2018: CH2018 – Climate Scenarios for Switzerland, Technical Report. National Centre for Climate Services, Zürich, 271
1013 pp, ISBN: 978-3-9525031-4-0, 2018.

1014 Chinita, M. J., Richardson, M., Teixeira, J., and Miranda, P. M. A.: Global mean frequency increases of daily and sub-daily
1015 heavy precipitation in ERA5, *Environ. Res. Lett.*, 16, 074035, <https://doi.org/10.1088/1748-9326/ac0caa>, 2021.

1016 Dalelane, C., Früh, B., Steger, C., and Walter, A.: A Pragmatic Approach to Build a Reduced Regional Climate Projection
1017 Ensemble for Germany Using the EURO-CORDEX 8.5 Ensemble, <https://doi.org/10.1175/JAMC-D-17-0141.1>, 2018.

1018 DCCEEW: National Climate Risk Assessment: Methodology. Department of Climate Change, Energy, the Environment and
1019 Water, <https://www.dceew.gov.au/climate-change/publications/national-climate-risk-assessment>, 2023.

1020 Dobler, A.: doblone/3DBC: Version 2023 (Versjon v2023), Zenodo, <https://doi.org/10.5281/zenodo.15260335>, 2025.

1021 Dobrowski, S. Z., Abatzoglou, J. T., Greenberg, J. A., and Schladow, S. G.: How much influence does landscape-scale
1022 physiography have on air temperature in a mountain environment?, *Agricultural and Forest Meteorology*, 149, 1751–1758,
1023 <https://doi.org/10.1016/j.agrformet.2009.06.006>, 2009.

1024 Doherty, J. and Skahill, B. E.: An advanced regularization methodology for use in watershed model calibration, *Journal of*
1025 *Hydrology*, 327, 564–577, <https://doi.org/10.1016/j.jhydrol.2005.11.058>, 2006.

1026 Dunn, R. J. H., Alexander, L. V., Donat, M. G., Zhang, X., Bador, M., Herold, N., Lippmann, T., Allan, R., Aguilar, E., Barry,
1027 A. A., Brunet, M., Caesar, J., Chagnaud, G., Cheng, V., Cinco, T., Durre, I., de Guzman, R., Htay, T. M., Wan Ibadullah, W.
1028 M., Bin Ibrahim, M. K. I., Khoshkam, M., Kruger, A., Kubota, H., Leng, T. W., Lim, G., Li-Sha, L., Marengo, J., Mbatha, S.,
1029 McGree, S., Menne, M., de los Milagros Skansi, M., Ngwenya, S., Nkrumah, F., Oonariya, C., Pabon-Caicedo, J. D., Panthou,
1030 G., Pham, C., Rahimzadeh, F., Ramos, A., Salgado, E., Salinger, J., Sané, Y., Sopaheluwakan, A., Srivastava, A., Sun, Y.,
1031 Timbal, B., Trachow, N., Trewin, B., van der Schrier, G., Vazquez-Aguirre, J., Vasquez, R., Villarroel, C., Vincent, L., Vischel,
1032 T., Vose, R., and Bin Hj Yussof, M. N.: Development of an Updated Global Land In Situ-Based Data Set of Temperature and
1033 Precipitation Extremes: HadEX3, *Journal of Geophysical Research: Atmospheres*, 125, e2019JD032263,
1034 <https://doi.org/10.1029/2019JD032263>, 2020.

1035 Dyrddal, A.V., Bakke, S.J., Hanssen-Bauer, I., Mayer, S., Nilsen, I.B., Nilsen, J.E.Ø., Paasche, Ø., Saloranta, T., Årthun, M.
1036 [editors]: Klima i Norge – kunnskapsgrunnlag for klimatilpassning oppdatert i 2025 (“Climate in Norway – knowledge base
1037 for climate adaptation updated in 2025”), NCCS Report 1/2025, Norwegian Centre for Climate Services, Oslo, Norway. (In
1038 Norwegian.). <https://doi.org/10.60839/4rgq-nn84>, 2025.

1039 Eaton, B., Gregory, J., Drach, B., Taylor, K., Hankin, S., Caron, J., Signell, R., Bentley, P., Rappa, G., Höck, H., Pamment,
1040 A., Juckes, M., Raspaud, M., Blower, J., Horne, R., Whiteaker, T., Blodgett, D., Zender, C., Lee, D., Hassell, D., Snow, A. D.,
1041 Kölling, T., Allured, D., Jelenak, A. Soerensen, A. M., Gaultier, L., Herlédan, S.: NetCDF Climate and Forecast (CF) Metadata
1042 Conventions (1.10). CF Community. <https://doi.org/10.5281/zenodo.14275561>, 2022.

1043 EEA (European Environment Agency): Energy Performance of Buildings Directive.
1044 [https://energy.ec.europa.eu/topics/energy-efficiency/energy-performance-buildings/energy-performance-buildings-](https://energy.ec.europa.eu/topics/energy-efficiency/energy-performance-buildings/energy-performance-buildings-directive_en)
1045 [directive_en](https://energy.ec.europa.eu/topics/energy-efficiency/energy-performance-buildings/energy-performance-buildings-directive_en), last access: 19 August 2025.

1046 Erlandsen, H. B., Beldring, S., Eisner, S., Hisdal, H., Huang, S., and Tallaksen, L. M.: Constraining the HBV model for robust
1047 water balance assessments in a cold climate, *Hydrology Research*, 52, 356–372, <https://doi.org/10.2166/nh.2021.132>, 2021.

1048 Eum, H.-I., Gupta, A., and Dibike, Y.: Effects of univariate and multivariate statistical downscaling methods on climatic and
1049 hydrologic indicators for Alberta, Canada, *Journal of Hydrology*, 588, 125065, <https://doi.org/10.1016/j.jhydrol.2020.125065>,
1050 2020.

1051 Eyring, V., Bony, S., Meehl, G. A., Senior, C. A., Stevens, B., Stouffer, R. J., and Taylor, K. E.: Overview of the Coupled
1052 Model Intercomparison Project Phase 6 (CMIP6) experimental design and organization, Geoscientific Model Development,
1053 9, 1937–1958, <https://doi.org/10.5194/gmd-9-1937-2016>, 2016.

1054 Fischer, A. M., Strassmann, K. M., Croci-Maspoli, M., Hama, A. M., Knutti, R., Kotlarski, S., Schär, C., Schnadt Poberaj, C.,
1055 Ban, N., Bavay, M., Beyerle, U., Bresch, D. N., Brönnimann, S., Burlando, P., Casanueva, A., Fatichi, S., Feigenwinter, I.,
1056 Fischer, E. M., Hirschi, M., Liniger, M. A., Marty, C., Medhaug, I., Peleg, N., Pickl, M., Raible, C. C., Rajczak, J., Rössler,
1057 O., Scherrer, S. C., Schwierz, C., Seneviratne, S. I., Skelton, M., Sørland, S. L., Spirig, C., Tschurr, F., Zeder, J., and Zubler,
1058 E. M.: Climate Scenarios for Switzerland CH2018 – Approach and Implications, Climate Services, 26, 100288,
1059 <https://doi.org/10.1016/j.cliser.2022.100288>, 2022.

1060 François, B., Vrac, M., Cannon, A. J., Robin, Y., and Allard, D.: Multivariate bias corrections of climate simulations: which
1061 benefits for which losses?, Earth System Dynamics, 11, 537–562, <https://doi.org/10.5194/esd-11-537-2020>, 2020.

1062 Franke, J.: Rainfall complexity in mountains, Nat. Clim. Chang., 14, 1223–1223, [https://doi.org/10.1038/s41558-024-02209-](https://doi.org/10.1038/s41558-024-02209-6)
1063 [6](https://doi.org/10.1038/s41558-024-02209-6), 2024.

1064 Gaarder, J.E., Tajet, H.T.T., Dobler, A., Hygen, H.O. and Kvande, T.: Future Climate Projections and Uncertainty Evaluations
1065 for Frost Decay Exposure Index in Norway. Buildings, 14(9), p.2873, <https://doi.org/10.3390/buildings14092873>, 2024

1066 Golding, N., Lambkin, K., Wilson, L., Troch, R. D., Fischer, A. M., Hygen, H. O., Hama, A. M., Dyrddal, A. V., Jamsin, E.,
1067 Termonia, P., and Hewitt, C.: Developing national frameworks for climate services: Experiences, challenges and learnings
1068 from across Europe, Climate Services, 37, 100530, <https://doi.org/10.1016/j.cliser.2024.100530>, 2025.

1069 Gjertsen, A.K. and Nilsen, J.E.: SAT-SKOG: Et skogkart basert på tolking av satellittbilder. Skog og landskap, rapport nr.
1070 23/2012, 54 pp, <http://hdl.handle.net/11250/2453917> 2012.

1071 Gu, G. and Adler, R. F.: Spatial Patterns of Global Precipitation Change and Variability during 1901–2010,
1072 <https://doi.org/10.1175/JCLI-D-14-00201.1>, 2015.

1073 Gudmundsson, L.: qmap: Statistical Transformations for Post-Processing Climate Model Output, version 1.0-6,
1074 <https://doi.org/10.32614/CRAN.package.qmap>, 2025.

1075 Gudmundsson, L., Bremnes, J. B., Haugen, J. E., and Engen-Skaugen, T.: Technical Note: Downscaling RCM precipitation to
1076 the station scale using statistical transformations – a comparison of methods, Hydrology and Earth System Sciences,
1077 16, 3383–3390, <https://doi.org/10.5194/hess-16-3383-2012>, 2012.

1078 Gudmundsson, L., Boulange, J., Do, H. X., Gosling, S. N., Grillakis, M. G., Koutroulis, A. G., Leonard, M., Liu, J., Müller
1079 Schmied, H., Papadimitriou, L., Pokhrel, Y., Seneviratne, S. I., Satoh, Y., Thiery, W., Westra, S., Zhang, X., and Zhao, F.:
1080 Globally observed trends in mean and extreme river flow attributed to climate change, *Science*, 371, 1159–1162,
1081 <https://doi.org/10.1126/science.aba3996>, 2021.

1082 Gutiérrez, J. M., Maraun, D., Widmann, M., Huth, R., Hertig, E., Benestad, R., Roessler, O., Wibig, J., Wilcke, R., Kotlarski,
1083 S., San Martín, D., Herrera, S., Bedia, J., Casanueva, A., Manzanas, R., Iturbide, M., Vrac, M., Dubrovsky, M., Ribalaya,
1084 J., Pórtoles, J., Rätty, O., Räisänen, J., Hingray, B., Raynaud, D., Casado, M. J., Ramos, P., Zerenner, T., Turco, M., Bosshard,
1085 T., Štěpánek, P., Bartholy, J., Pongracz, R., Keller, D. E., Fischer, A. M., Cardoso, R. M., Soares, P. M. M., Czernecki, B.,
1086 and Pagé, C.: An intercomparison of a large ensemble of statistical downscaling methods over Europe: Results from the
1087 VALUE perfect predictor cross-validation experiment, *International Journal of Climatology*, 39, 3750–3785,
1088 <https://doi.org/10.1002/joc.5462>, 2019.

1089 Hanssen-Bauer, I., Benestad, R.E., Lutz, J., Vikhamar-Schuler, D., Svyashchennikov, P. and Førland, E.J: Comparative
1090 Analyses of Local Historical and Future Climate Conditions Important for Reindeer Herding in Finnmark, Norway and the
1091 Yamal Nenets Autonomous Okrug, Russia. In: Mathiesen, S.D., Eira, I.M.G., Turi, E.I., Oskal, A., Pogodaev, M., Tonkopeeva,
1092 M. (eds) Reindeer Husbandry. Springer Polar Sciences. Springer, Cham. https://doi.org/10.1007/978-3-031-17625-8_8, 2022

1093 Hanssen-Bauer, I., E.J.Førland, I.Haddeland, H.Hisdal, S.Mayer, A.Nesje, J.E.Ø.Nilsen, S.Sandven, A.B.Sandø, A.Sorteberg
1094 and B.Ådlandsvik: Klima i Norge 2100 – Kunnskapsgrunnlag for klimatilpasning oppdatert i 2015. Norsk Klimaservicesenter,
1095 NCCS Report 2/2015, 203pp, ISSN: 2387-3027, 2015.

1096 Hawkins, E. and Sutton, R.: The potential to narrow uncertainty in projections of regional precipitation change, *Clim Dyn*, 37,
1097 407–418, <https://doi.org/10.1007/s00382-010-0810-6>, 2011.

1098 Hersbach, H., Bell, B., Berrisford, P., Hirahara, S., Horányi, A., Muñoz-Sabater, J., Nicolas, J., Peubey, C., Radu, R., Schepers,
1099 D., Simmons, A., Soci, C., Abdalla, S., Abellan, X., Balsamo, G., Bechtold, P., Biavati, G., Bidlot, J., Bonavita, M., De Chiara,
1100 G., Dahlgren, P., Dee, D., Diamantakis, M., Dragani, R., Flemming, J., Forbes, R., Fuentes, M., Geer, A., Haimberger, L.,
1101 Healy, S., Hogan, R. J., Hólm, E., Janisková, M., Keeley, S., Laloyaux, P., Lopez, P., Lupu, C., Radnoti, G., de Rosnay, P.,
1102 Rozum, I., Vamborg, F., Villaume, S., and Thépaut, J.-N.: The ERA5 global reanalysis, *Quarterly Journal of the Royal
1103 Meteorological Society*, 146, 1999–2049, <https://doi.org/10.1002/qj.3803>, 2020.

1104 Hisdal, H., Vikhamar-Schuler, D., Førland, E., and Nilsen, I.: Klimaprofiler for fylker. (“Climate factsheets for counties”).
1105 NCCS Report 2/2021, Norwegian Centre for Climate Services, Oslo, Norway. (In Norwegian).
1106 https://klimaservicesenter.no/kss/rapporter/rapporter-og-publikasjoner_2 , 2021.

- 1107 Huang, S., Eisner, S., Magnusson, J. O., Lussana, C., Yang, X., and Beldring, S.: Improvements of the spatially distributed
1108 hydrological modelling using the HBV model at 1 km resolution for Norway, *Journal of Hydrology*, 577, 123585,
1109 <https://doi.org/10.1016/j.jhydrol.2019.03.051>, 2019.
- 1110 Huang, S., Eisner, S., Haddeland, I., and Tadege Mengistu, Z.: Evaluation of two new-generation global soil databases for
1111 macro-scale hydrological modelling in Norway, *Journal of Hydrology*, 610, 127895,
1112 <https://doi.org/10.1016/j.jhydrol.2022.127895>, 2022.
- 1113 Huang, S., Eisner, S., Wong, W. K., and Cattaneo, N.: The potential impacts of climate and forest changes on streamflow for
1114 micro-, meso- and macro-scale catchments in Norway, *Journal of Hydrology: Regional Studies*, 57, 102147,
1115 <https://doi.org/10.1016/j.ejrh.2024.102147>, 2025a.
- 1116 Huang, S., Haddeland, I., Lussana, C., Dobler, A., and Tveito, O.E.: Daily climate and hydrological reference data for Norway
1117 [Data set]. Dataset published 2025 via Norwegian Meteorological Institute, <https://doi.org/10.21343/gbq0-4t97>, 2025b.
- 1118 Huang, S., Wong, W.K., Tveito, O.E., Haddeland, I.: Impacts of empirical and physical evaporation methods on changes in
1119 hydrological components and drought indices under climate change scenarios, *Hydrology Research*, doi: 10.2166/nh.2026.220,
1120 2026.
- 1121 Hundecha, Y., Sunyer, M. A., Lawrence, D., Madsen, H., Willems, P., Bürger, G., Kriaučiūnienė, J., Loukas, A., Martinkova,
1122 M., Osuch, M., Vasiliades, L., von Christerson, B., Vormoor, K., and Yücel, I.: Inter-comparison of statistical downscaling
1123 methods for projection of extreme flow indices across Europe, *Journal of Hydrology*, 541, 1273–1286,
1124 <https://doi.org/10.1016/j.jhydrol.2016.08.033>, 2016.
- 1125 Huss, M., Juvet, G., Farinotti, D., and Bauder, A.: Future high-mountain hydrology: a new parameterization of glacier retreat,
1126 *Hydrology and Earth System Sciences*, 14, 815–829, <https://doi.org/10.5194/hess-14-815-2010>, 2010.
- 1127 Hübener, H., Hoffmann, P., Keuler, K., Pfeifer, S., Ramthun, H., Spekat, A., Steger, C., and Warrach-Sagi, K.: Deriving user-
1128 informed climate information from climate model ensemble results, in: *Advances in Science and Research*, 16th EMS Annual
1129 Meeting & 11th European Conference on Applied Climatology (ECAC) -, 261–269, <https://doi.org/10.5194/asr-14-261-2017>,
1130 2017.
- 1131 IPCC: Climate Change 2021: The Physical Science Basis. Contribution of Working Group I to the Sixth Assessment Report
1132 of the Intergovernmental Panel on Climate Change [Masson-Delmotte, V., P. Zhai, A. Pirani, S.L. Connors, C. Péan, S. Berger,
1133 N. Caud, Y. Chen, L. Goldfarb, M.I. Gomis, M. Huang, K. Leitzell, E. Lonnoy, J.B.R. Matthews, T.K. Maycock, T. Waterfield,

- 1134 O. Yelekçi, R. Yu, and B. Zhou (eds.]. Cambridge University Press, Cambridge, United Kingdom and New York, NY, USA,
1135 In press, doi:[10.1017/9781009157896](https://doi.org/10.1017/9781009157896), 2021.
- 1136 Jacob, D., Petersen, J., Eggert, B., Alias, A., Christensen, O. B., Bouwer, L. M., Braun, A., Colette, A., Déqué, M., Georgievski,
1137 G., Georgopoulou, E., Gobiet, A., Menut, L., Nikulin, G., Haensler, A., Hempelmann, N., Jones, C., Keuler, K., Kovats, S.,
1138 Kröner, N., Kotlarski, S., Kriegsmann, A., Martin, E., van Meijgaard, E., Moseley, C., Pfeifer, S., Preuschmann, S.,
1139 Radermacher, C., Radtke, K., Rechid, D., Rounsevell, M., Samuelsson, P., Somot, S., Soussana, J.-F., Teichmann, C.,
1140 Valentini, R., Vautard, R., Weber, B., and Yiou, P.: EURO-CORDEX: new high-resolution climate change projections for
1141 European impact research, *Reg Environ Change*, 14, 563–578, <https://doi.org/10.1007/s10113-013-0499-2>, 2014.
- 1142 Jacob, D., Teichmann, C., Sobolowski, S., Katragkou, E., Anders, I., Belda, M., Benestad, R., Boberg, F., Buonomo, E.,
1143 Cardoso, R. M., Casanueva, A., Christensen, O. B., Christensen, J. H., Coppola, E., De Cruz, L., Davin, E. L., Dobler, A.,
1144 Domínguez, M., Fealy, R., Fernandez, J., Gaertner, M. A., García-Díez, M., Giorgi, F., Gobiet, A., Goergen, K., Gómez-
1145 Navarro, J. J., Alemán, J. J. G., Gutiérrez, C., Gutiérrez, J. M., Güttler, I., Haensler, A., Halenka, T., Jerez, S., Jiménez-
1146 Guerrero, P., Jones, R. G., Keuler, K., Kjellström, E., Knist, S., Kotlarski, S., Maraun, D., van Meijgaard, E., Mercogliano, P.,
1147 Montávez, J. P., Navarra, A., Nikulin, G., de Noblet-Ducoudré, N., Panitz, H.-J., Pfeifer, S., Piazza, M., Pichelli, E.,
1148 Pietikäinen, J.-P., Prein, A. F., Preuschmann, S., Rechid, D., Rockel, B., Romera, R., Sánchez, E., Sieck, K., Soares, P. M. M.,
1149 Somot, S., Srnec, L., Sørland, S. L., Termonia, P., Truhetz, H., Vautard, R., Warrach-Sagi, K., and Wulfmeyer, V.: Regional
1150 climate downscaling over Europe: perspectives from the EURO-CORDEX community, *Reg Environ Change*, 20, 51,
1151 <https://doi.org/10.1007/s10113-020-01606-9>, 2020.
- 1152 Katragkou, E., Sobolowski, S.P., Teichmann, C., Solmon, F., Pavlidis, V., Rechid, D., Hoffmann, P., Fernández, J., Nikulin,
1153 G. and Jacob, D.: Delivering an improved framework for the new generation of CMIP6-driven EURO-CORDEX regional
1154 climate simulations. *Bulletin of the American Meteorological Society*, 105(6), pp.E962-E974, [https://doi.org/10.1175/BAMS-](https://doi.org/10.1175/BAMS-D-23-0131.1)
1155 [D-23-0131.1](https://doi.org/10.1175/BAMS-D-23-0131.1), 2024.
- 1156 Kay, A. L.: A comparison of hydrological impacts from two ensembles of regional climate projections with a range of climate
1157 sensitivities, *Reg Environ Change*, 25, 89, <https://doi.org/10.1007/s10113-025-02426-5>, 2025.
- 1158 Kundzewicz, Z. W., Krysanova, V., Dankers, R., Hirabayashi, Y., Kanae, S., Hattermann, F. F., Huang, S., Milly, P. C. D.,
1159 Stoffel, M., Driessen, P. P. J., Matczak, P., Quevauviller, P., and Schellnhuber, H.-J.: Differences in flood hazard projections
1160 in Europe – their causes and consequences for decision making, *Hydrological Sciences Journal*, 62, 1–14,
1161 <https://doi.org/10.1080/02626667.2016.1241398>, 2017.

- 1162 Kuya, E. K., Hanssen-Bauer, I., Mayer, S., and Heiberg, H.: Projected changes of rain, sleet, and snowfall in Norway, Norsk
1163 Geografisk Tidsskrift - Norwegian Journal of Geography, 78, 73–87, <https://doi.org/10.1080/00291951.2024.2360409>, 2024.
- 1164 Lafferty, D. C. and Sriver, R. L.: Downscaling and bias-correction contribute considerable uncertainty to local climate
1165 projections in CMIP6, npj Clim Atmos Sci, 6, 158, <https://doi.org/10.1038/s41612-023-00486-0>, 2023.
- 1166 Lawrence, D.: Uncertainty introduced by flood frequency analysis in projections for changes in flood magnitudes under a
1167 future climate in Norway. Journal of Hydrology: Regional Studies 28:100675, <https://doi.org/10.1016/j.ejrh.2020.100675>,
1168 2020.
- 1169 Lhotka, O., Plavcová, E. and Beranová, R.: Future Changes in Day-to-Day Precipitation Variability in Europe. Journal of
1170 Hydrometeorology 25, 8, <https://doi.org/10.1175/JHM-D-23-0206.1>, 2024.
- 1171 Li, H., Beldring, S., Xu, C.-Y., Huss, M., Melvold, K., and Jain, S. K.: Integrating a glacier retreat model into a hydrological
1172 model – Case studies of three glacierised catchments in Norway and Himalayan region, Journal of Hydrology, 527, 656–667,
1173 <https://doi.org/10.1016/j.jhydrol.2015.05.017>, 2015.
- 1174 Li, L., Wang, B., Feng, P., Jägermeyr, J., Asseng, S., Müller, C., Macadam, I., Liu, D. L., Waters, C., Zhang, Y., He, Q., Shi,
1175 Y., Chen, S., Guo, X., Li, Y., He, J., Feng, H., Yang, G., Tian, H., and Yu, Q.: The optimization of model ensemble composition
1176 and size can enhance the robustness of crop yield projections, Commun Earth Environ, 4, 362, [https://doi.org/10.1038/s43247-
1177 023-01016-9](https://doi.org/10.1038/s43247-023-01016-9), 2023.
- 1178 Liersch, S., Drews, M., Pilz, T., Salack, S., Sietz, D., Aich, V., A D Larsen, M., Gädeke, A., Halsnæs, K., Thiery, W., Huang,
1179 S., Lobanova, A., Koch, H., and Hattermann, F. F.: One simulation, different conclusions—the baseline period makes the
1180 difference!, Environ. Res. Lett., 15, 104014, <https://doi.org/10.1088/1748-9326/aba3d7>, 2020.
- 1181 Lussana, C: seNorge observational gridded datasets, MET report 7-2020, [https://www.met.no/publikasjoner/met-report/met-
1182 report-2020/_attachment/download/9f79d391-62d8-4fc1-a61a-
1183 9f0e7f1de389:8c74ebf2118593aa75272e6aff416ce66f86e73f/MET-report-07-2020.pdf](https://www.met.no/publikasjoner/met-report/met-report-2020/_attachment/download/9f79d391-62d8-4fc1-a61a-9f0e7f1de389:8c74ebf2118593aa75272e6aff416ce66f86e73f/MET-report-07-2020.pdf), 2020.
- 1184 Lussana, C., Tveito, O. E., Dobler, A., and Tunheim, K.: seNorge_2018, daily precipitation, and temperature datasets over
1185 Norway, Earth System Science Data, 11, 1531–1551, <https://doi.org/10.5194/essd-11-1531-2019>, 2019.
- 1186 Lutz, J., Hanssen-Bauer, I., Tveito, O. E. and Dobler, A.: Precipitation variability in Norway 1961–2020. MET-report 01-
1187 2024, [https://www.met.no/publikasjoner/met-report/_attachment/download/f5ba4d69-dba2-4eb6-bed9-
1188 0189178b5e7a:ba4f4974e503f9509d33f101efc40145b47a59e6/MET%20report%201%202024.pdf](https://www.met.no/publikasjoner/met-report/_attachment/download/f5ba4d69-dba2-4eb6-bed9-0189178b5e7a:ba4f4974e503f9509d33f101efc40145b47a59e6/MET%20report%201%202024.pdf), 2024.

- 1189 Majasalmi, T., Eisner, S., Astrup, R., Fridman, J., and Bright, R. M.: An enhanced forest classification scheme for modeling
1190 vegetation–climate interactions based on national forest inventory data, *Biogeosciences*, 15, 399–412,
1191 <https://doi.org/10.5194/bg-15-399-2018>, 2018.
- 1192 Maraun, D.: Bias Correction, Quantile Mapping, and Downscaling: Revisiting the Inflation Issue. *Journal of Climate*, 26,
1193 2137–2143, <https://doi.org/10.1175/jcli-d-12-00821.1>, 2013.
- 1194 Maraun, D. and Widmann, M.: *Statistical Downscaling and Bias Correction for Climate Research*. Cambridge University
1195 Press, 347 pp, 2018.
- 1196 Martinich, J. and Crimmins, A.: Climate damages and adaptation potential across diverse sectors of the United States, *Nature*
1197 *Climate Change*, 9, 397-404, 2019.
- 1198 Matiu, M., Napoli, A., Kotlarski, S., Zardi, D., Bellin, A., and Majone, B.: Elevation-dependent biases of raw and bias-
1199 adjusted EURO-CORDEX regional climate models in the European Alps, *Climate Dynamics*,
1200 <https://doi.org/10.1007/s00382-024-07376-y>, 2024.
- 1201 Mayer, S., Khasandi Kuya, E., Antonsen, K., Abegg, B., and Hanssen-Bauer, I.: Warmer and wetter: Outlining climate services
1202 for snow-dependent tourism in Norway – The case of Lofoten, *Climate Services*, 32, 100405,
1203 <https://doi.org/10.1016/j.cliser.2023.100405>, 2023.
- 1204 McAfee, S. A.: Methodological differences in projected potential evapotranspiration, *Climatic Change*, 120, 915–930,
1205 <https://doi.org/10.1007/s10584-013-0864-7>, 2013.
- 1206 McSweeney, C. F., Jones, R. G., Lee, R. W., and Rowell, D. P.: Selecting CMIP5 GCMs for downscaling over multiple
1207 regions, *Clim Dyn*, 44, 3237–3260, <https://doi.org/10.1007/s00382-014-2418-8>, 2015.
- 1208 Mehrotra, R. and Sharma, A.: A Resampling Approach for Correcting Systematic Spatiotemporal Biases for Multiple Variables
1209 in a Changing Climate, *Water Resources Research*, 55, 754–770, <https://doi.org/10.1029/2018WR023270>, 2019.
- 1210 Meyer, J., Kohn, I., Stahl, K., Hakala, K., Seibert, J., and Cannon, A. J.: Effects of univariate and multivariate bias correction
1211 on hydrological impact projections in alpine catchments, *Hydrol. Earth Syst. Sci.*, 23, 1339–1354, [https://doi.org/10.5194/hess-](https://doi.org/10.5194/hess-23-1339-2019)
1212 [23-1339-2019](https://doi.org/10.5194/hess-23-1339-2019), 2019.
- 1213 Moriasi, D. N., Arnold, J. G., Liew, M. W. V., Bingner, R. L., Harmel, R. D., and Veith, T. L.: Model Evaluation Guidelines
1214 for Systematic Quantification of Accuracy in Watershed Simulations, *Transactions of the ASABE*, 50, 885–900,
1215 <https://doi.org/10.13031/2013.23153>, 2007.

- 1216 Müller, M., Homleid, M., Ivarsson, K.-I., Køltzow, M. A. Ø., Lindskog, M., Midtbø, K. H., Andrae, U., Aspelien, T., Berggren,
1217 L., Bjørge, D., Dahlgren, P., Kristiansen, J., Randriamampianina, R., Ridal, M., and Vignes, O.: AROME-MetCoOp: A Nordic
1218 Convective-Scale Operational Weather Prediction Model, <https://doi.org/10.1175/WAF-D-16-0099.1>, 2017.
- 1219 Nash, J.E. and Sutcliffe, J.V.: River flow forecasting through conceptual models part I -A discussion of principles, *J Hydrol*,
1220 10, 282–290, 1970.
- 1221 Nilsen, I. B., Hanssen-Bauer, I., Tveito, O. E., and Wong, W. K.: Projected changes in days with zero-crossings for Norway,
1222 *International Journal of Climatology*, 41, 2173–2188, <https://doi.org/10.1002/joc.6913>, 2021.
- 1223 Nilsen, I. B., Hanssen-Bauer, I., Dyrddal, A. V., Hisdal, H., Lawrence, D., Haddeland, I., and Wong, W. K.: From Climate
1224 Model Output to Actionable Climate Information in Norway, *Front. Clim.*, 4, <https://doi.org/10.3389/fclim.2022.866563>,
1225 2022.
- 1226 Norwegian Government: Statlige Planretningslinjer for klima- og energi. (“government guidelines on climate and renergy”),
1227 available online at: <https://lovdata.no/dokument/SF/forskrift/2024-12-20-3359> (accessed December 06. October 2025), 2024.
- 1228 Padrón, R. S., Gudmundsson, L., Decharme, B., Ducharne, A., Lawrence, D. M., Mao, J., Peano, D., Krinner, G., Kim, H.,
1229 and Seneviratne, S. I.: Observed changes in dry-season water availability attributed to human-induced climate change, *Nat.*
1230 *Geosci.*, 13, 477–481, <https://doi.org/10.1038/s41561-020-0594-1>, 2020.
- 1231 Paz, S.M. and Willems, P.: Uncovering the strengths and weaknesses of an ensemble of quantile mapping methods for
1232 downscaling precipitation change in Southern Africa. *J. Hydrol. -Reg. Stud.* 41, 101104,
1233 <https://doi.org/10.1016/j.ejrh.2022.101104>, 2022.
- 1234 Peter, J., Vogel, E., Sharples, W., Bende-Michl, U., Wilson, L., Hope, P., Dowdy, A., Kociuba, G., Srikanthan, S., Duong, V.
1235 C., Roussis, J., Matic, V., Khan, Z., Oke, A., Turner, M., Baron-Hay, S., Johnson, F., Mehrotra, R., Sharma, A., Thatcher, M.,
1236 Azarvinand, A., Thomas, S., Boschat, G., Donnelly, C., and Argent, R.: Continental-scale bias-corrected climate and
1237 hydrological projections for Australia, *Geoscientific Model Development*, 17, 2755–2781, [https://doi.org/10.5194/gmd-17-
1238 2755-2024](https://doi.org/10.5194/gmd-17-2755-2024), 2024.
- 1239 Pirk, N., Aalstad, K., Yilmaz, Y. A., Vatne, A., Popp, A. L., Horvath, P., Bryn, A., Vollsnes, A. V., Westermann, S., Berntsen,
1240 T. K., Stordal, F., and Tallaksen, L. M.: Snow–vegetation–atmosphere interactions in alpine tundra, *Biogeosciences*, 20, 2031–
1241 2047, <https://doi.org/10.5194/bg-20-2031-2023>, 2023.

- 1242 Pourmokhtarian, A., Driscoll, C. T., Campbell, J. L., Hayhoe, K., and Stoner, A. M. K.: The effects of climate downscaling
1243 technique and observational data set on modeled ecological responses, *Ecological Applications*, 26, 1321–1337,
1244 <https://doi.org/10.1890/15-0745>, 2016.
- 1245 Reistad, M., Øyvind Breivik, Haakenstad, H., Aarnes, O. J., Furevik, B. R., and Bidlot, J.-R.: A high-resolution hindcast of
1246 wind and waves for the North Sea, the Norwegian Sea, and the Barents Sea, *J. Geophys. Res.*, 116,
1247 <https://doi.org/10.1029/2010JC006402>, 2011.
- 1248 Reyniers, N., Zha, Q., Addor, N., Osborn, T. J., Forstnhäusler, N., and He, Y.: Two sets of bias-corrected regional UK Climate
1249 Projections 2018 (UKCP18) of temperature, precipitation and potential evapotranspiration for Great Britain, *Earth System
1250 Science Data*, 17, 2113–2133, <https://doi.org/10.5194/essd-17-2113-2025>, 2025.
- 1251 Rössler, O., Fischer, A. M., Huebener, H., Maraun, D., Benestad, R. E., Christodoulides, P., Soares, P. M. M., Cardoso, R. M.,
1252 Pagé, C., Kanamaru, H., Kreienkamp, F., and Vlachogiannis, D.: Challenges to link climate change data provision and user
1253 needs: Perspective from the COST-action VALUE, *International Journal of Climatology*, 39, 3704–3716,
1254 <https://doi.org/10.1002/joc.5060>, 2019.
- 1255 Statistics Norway: [Land use and land cover – SSB](#), last accessed on 27.03.2025, 2025.
- 1256 Schumacher, D.L., Singh, J., Hauser, M., Fischer, E.M., Wild, M. and Seneviratne, S.I.: Exacerbated summer European
1257 warming not captured by climate models neglecting long-term aerosol changes. *Communications Earth & Environment*, 5(1),
1258 p.182, <https://doi.org/10.1038/s43247-024-01332-8>, 2024.
- 1259 Sobolowski, S., Somot, S., Fernandez, J., Evin, G., Brands, S., Maraun, D., Kotlarski, S., Jury, M., Benestad, R.E., Teichmann,
1260 C. and Christensen, O.B.: GCM Selection and Ensemble Design: Best Practices and Recommendations from the EURO-
1261 CORDEX Community, *Bulletin of the American Meteorological Society*, 106(9), pp.E1834-E1850,
1262 <https://doi.org/10.1175/BAMS-D-23-0189.1>, 2025.
- 1263 Tam, B., Bonsal, B., Zhang, X., Zhang, Q., and Rong, R.: Assessing Potential Evapotranspiration Methods in Future Drought
1264 Projections across Canada, *Atmosphere-Ocean*, 62, 193–205, <https://doi.org/10.1080/07055900.2023.2288632>, 2024.
- 1265 Tang, J., Niu, X., Wang, S., Gao, H., Wang, X., and Wu, J.: Statistical downscaling and dynamical downscaling of regional
1266 climate in China: Present climate evaluations and future climate projections, *Journal of Geophysical Research: Atmospheres*,
1267 121, 2110–2129, <https://doi.org/10.1002/2015JD023977>, 2016.

- 1268 Taylor, K. E., Stouffer, R. J., and Meehl, G. A.: An overview of CMIP5 and the experiment design, *B. Am. Meteorol. Soc.*,
1269 93, 485–498, <https://doi.org/10.1175/BAMS-D-11-00094.1>, 2012.
- 1270 Thorarinsdottir, T. L., Gneiting, T., and Gissibl, N.: Using proper divergence functions to evaluate climate models. *SIAM-*
1271 *ASA J. Uncertainty Quantif.*, 1, 522–534, <https://doi.org/10.1137/130907550>, 2013.
- 1272 Tong, Y., Gao, X., Han, Z., Xu, Y. and Giorgi, F.: Bias correction of temperature and precipitation over China for RCM
1273 simulations using the QM and QDM methods, *Climate Dynamics* 57, 1425–1443, [https://doi.org/10.1007/s00382-020-05447-](https://doi.org/10.1007/s00382-020-05447-4)
1274 4, 2021.
- 1275 Tveito, O. E.: Norwegian standard climate normals 1991-2020 – the methodological approach, MET report 5 2021,
1276 [https://www.met.no/publikasjoner/met-report/met-report-2021/_/attachment/download/31bb0160-d8cf-4a2b-9646-](https://www.met.no/publikasjoner/met-report/met-report-2021/_/attachment/download/31bb0160-d8cf-4a2b-9646-4df6f5904059:3ac4fec6cf3fb7919ae42db2b63ad8e8b9e6a6/METreport%2005_2021_New_Norwegian_standard_climate_normals_1991_2020-signert.pdf)
1277 4df6f5904059:3ac4fec6cf3fb7919ae42db2b63ad8e8b9e6a6/METreport%2005_2021_New_Norwegian_standard_climate_
1278 normals_1991_2020-signert.pdf, 2021.
- 1279 Vautard, R., Kadyrov, N., Iles, C., Boberg, F., Buonomo, E., Bülow, K., Coppola, E., Corre, L., van Meijgaard, E.,
1280 Nogherotto, R., Sandstad, M., Schwingshackl, C., Somot, S., Aalbers, E., Christensen, O. B., Ciarlo, J. M., Demory, M.-E.,
1281 Giorgi, F., Jacob, D., Jones, R. G., Keuler, K., Kjellström, E., Lenderink, G., Levavasseur, G., Nikulin, G., Sillmann, J.,
1282 Solidoro, C., Sørland, S. L., Steger, C., Teichmann, C., Warrach-Sagi, K., and Wulfmeyer, V.: Evaluation of the Large EURO-
1283 CORDEX Regional Climate Model Ensemble, *Journal of Geophysical Research: Atmospheres*, 126, e2019JD032344,
1284 <https://doi.org/10.1029/2019JD032344>, 2021.
- 1285 Vetter, T., Reinhardt, J., Flörke, M., van Griensven, A., Hattermann, F., Huang, S., Koch, H., Pechlivanidis, I. G., Plötner, S.,
1286 Seidou, O., Su, B., Vervoort, R. W., and Krysanova, V.: Evaluation of sources of uncertainty in projected hydrological changes
1287 under climate change in 12 large-scale river basins, *Climatic Change*, 141, 419–433, [https://doi.org/10.1007/s10584-016-1794-](https://doi.org/10.1007/s10584-016-1794-y)
1288 [y](https://doi.org/10.1007/s10584-016-1794-y), 2017.
- 1289 Wang, X. and Liu, L.: The Impacts of Climate Change on the Hydrological Cycle and Water Resource Management, *Water*,
1290 15, 2342, <https://doi.org/10.3390/w15132342>, 2023.
- 1291 Wilkinson, M. D., Dumontier, M., Aalbersberg, Ij. J., Appleton, G., Axton, M., Baak, A., Blomberg, N., Boiten, J.-W., da
1292 Silva Santos, L. B., Bourne, P. E., Bouwman, J., Brookes, A. J., Clark, T., Crosas, M., Dillo, I., Dumon, O., Edmunds, S.,
1293 Evelo, C. T., Finkers, R., Gonzalez-Beltran, A., Gray, A. J. G., Groth, P., Goble, C., Grethe, J. S., Heringa, J., 't Hoen, P. A.
1294 C., Hooft, R., Kuhn, T., Kok, R., Kok, J., Lusher, S. J., Martone, M. E., Mons, A., Packer, A. L., Persson, B., Rocca-Serra, P.,
1295 Roos, M., van Schaik, R., Sansone, S.-A., Schultes, E., Sengstag, T., Slater, T., Strawn, G., Swertz, M. A., Thompson, M., van
1296 der Lei, J., van Mulligen, E., Velterop, J., Waagmeester, A., Wittenburg, P., Wolstencroft, K., Zhao, J., and Mons, B.: The

1297 FAIR Guiding Principles for scientific data management and stewardship, *Sci Data*, 3, 160018,
1298 <https://doi.org/10.1038/sdata.2016.18>, 2016.

1299 Wolff, M. A., Isaksen, K., Petersen-Øverleir, A., Ødemark, K., Reitan, T., and Brækkan, R.: Derivation of a new continuous
1300 adjustment function for correcting wind-induced loss of solid precipitation: results of a Norwegian field study, *Hydrology and*
1301 *Earth System Sciences*, 19, 951–967, <https://doi.org/10.5194/hess-19-951-2015>, 2015.

1302 Wong, W.K., Dobler, A., Huang, S., Beldring, S., Melvold, K., Ruan, G.: Daily bias-adjusted climate (COR-BA-2025) and
1303 hydrological (distHBV-COR-BA-2025) projections for Norway [Data set]. Dataset published 2025 via Norwegian
1304 Meteorological Institute <https://doi.org/10.21343/0k90-6w67>, 2025

1305 Wong, W.K., Haddeland, I., Lawrence, D., and Beldring, S.: Gridded 1x1 km climate and hydrological projections for Norway.
1306 NVE Report No. 59, Norwegian Water Resources and Energy Directorate, Oslo, Norway, 2016.

1307 Yilmaz, K. K., Gupta, H. V., and Wagener, T.: A process-based diagnostic approach to model evaluation: Application to the
1308 NWS distributed hydrologic model, *Water Resources Research*, 44, <https://doi.org/10.1029/2007WR006716>, 2008.

1309 Yuan, Q., Thorarinsdottir, T. L., Beldring, S., Wong, W. K., Huang, S., and Xu, C.-Y.: New Approach for Bias Correction and
1310 Stochastic Downscaling of Future Projections for Daily Mean Temperatures to a High-Resolution Grid, *J. Appl. Meteorol.*
1311 *Clim.*, 58, 2617–2632, <https://doi.org/10.1175/JAMC-D-19-0086.1>, 2019.

1312 Yuan Q., Thorarinsdottir T.L., Beldring S., Wong W.K., and Xu C.-Y.: Bridging the scale gap: obtaining high-resolution
1313 stochastic simulations of gridded daily precipitation in a future climate, *Hydrol. Earth Syst. Sci.*, 25 (9), pp. 5259-5275,
1314 <https://doi.org/10.5194/hess-25-5259-2021>, 2021.

1315 Zhang, H., Chapman, S., Trancoso, R., Toombs, N. and Syktus, J.: Assessing the impact of bias correction approaches on
1316 climate extremes and the climate change signal, *Meteorol. Appl.*, 31, 1-18, <https://doi.org/10.1002/met.2204>, 2024.

1317 Zhang, L., Xu, Y., Meng, C., Li, X., Liu, H., and Wang, C.: Comparison of Statistical and Dynamic Downscaling Techniques
1318 in Generating High-Resolution Temperatures in China from CMIP5 GCMs, <https://doi.org/10.1175/JAMC-D-19-0048.1>,
1319 2020.

1320